NANO · MICRO small
www.small-journal.com

In Situ Nitric Oxide Generating Nano-Bioactive Glass-Based Coatings and Its Therapeutic Ion Release toward Attenuating Implant-Associated Fibrosis and Infection

*Joseph Christakiran Moses, Aasma Sapkota, Yi Wu, Isabel Martinez, Hitesh Handa, and Elizabeth J. Brisbois**

Nitric oxide (NO) is a potent gasotransmitter that exhibits a pleiotropic effect in regulating homeostasis and pathophysiology. Though it is a versatile biomaterial, silicone-based devices are still challenged by implant-associated infections and fibrous capsule formation complications. Here, a NO-generating (NOgen) interface is developed from copper or strontium-doped mesoporous bioactive glass-based coating on silicone substrates to facilitate metal-ion catalysis of endogenous S-nitrosothiols. The copper or strontium-based interfaces can generate physiologically relevant NO levels, which have bactericidal and antithrombotic effects to combat implant-associated early onsite infection and thrombosis. The NO generated in tandem with the low therapeutic release of strontium ions from the NOgen interface regulates cellular fate pertaining to fibroblasts, macrophages, and endothelial cells. Strontium suppresses the collagen expression and migration of activated fibroblasts while favoring M_2 phenotype bias in macrophages. Differential NO flux observed over time from NOgen interfaces helps switch macrophages from proinflammatory M_1 phenotype to M_2 anti-inflammatory phenotype. Moreover, the synergistic effect of leachate and NO generated by the silicone substrate demonstrates a proangiogenic effect by aiding endothelial network maturation in vitro. Thus, the multifunctional features of the developed strontium-doped bioactive glass-based coating hold promise in regulating local immune-micromilieu and attenuating implant-associated fibrosis of silicone-based implantable devices.

1. Introduction

Silicone-based (—[O—Si$(CH_3)_2$]$_n$—) biomaterials are the most commonly employed biomaterials for implantable device applications owing to their bio-inertness, anti-adhesiveness, and low cytotoxicity. This has led to the use of silicone-based devices in long-term (months to years) applications, such as defect fillers in lumpectomy or muscle atrophy conditions for augmentation or restoration of the defects and as tracheobronchial or vascular stents. Silicone-based devices have also been used for short-term (weeks to months) applications, such as in catheters and totally implanted venous access ports (TIVADs). Though being a versatile biomaterial, silicone-based devices are still challenged by complications relating to implant-associated infections and fibrous capsule formation. Chronic infections associated with such implantable devices occur at an incidence rate of ≈5%, but the impending risk factors relating to antimicrobial resistance and the vulnerability to cause serious complications in immunocompromised and elderly patients exacerbate this low-frequency number.[1] Similarly, a 10.6% incidence rate of fibrous capsule formation is noticed in silicone implants used for augmentative or restoration procedures, leading to pain, discomfort at the implant site, and, ultimately, device failure.[2,3]

As with any foreign device implanted in the body, it evokes the foreign body response, a sequential cascade of biomolecular and cellular events that decides the fate of the implanted biomaterial (Figure S1, Electronic Supporting Information). Soon after implantation, the biomaterial surface is crowded by the blood proteins, followed by the immune cells engaging with the surface. If the material surface is not conducive, it triggers the activation of the chronic inflammatory phase, which involves the activation of macrophages, formation of foreign body giant cells, and myofibroblast phenotype conversion, leading to fibrous encapsulation. Pertinent to note here is that the fibroblast activation and its phenotype control are dependent on the inflammatory environment, which is closely regulated by macrophage-fibroblast crosstalk.[4] The presence of implant-associated

J. C. Moses, A. Sapkota, Y. Wu, I. Martinez, H. Handa, E. J. Brisbois
School of Chemical
Materials and Biomedical Engineering
College of Engineering
University of Georgia
Athens, GA 30602, USA
E-mail: ejbrisbois@uga.edu
H. Handa
Pharmaceutical and Biomedical Sciences Department
College of Pharmacy
University of Georgia
Athens, GA 30602, USA
The ORCID identification number(s) for the author(s) of this article can be found under https://doi.org/10.1002/smll.202411984

DOI: 10.1002/smll.202411984

opportunistic microbes can further worsen the chronic inflammation phase, divulging out as an infection at the implant site. Pharmacological interventions involve the systemic administration of immunomodulatory drugs or antibiotics to curtail these complications. The use of broad-spectrum anti-inflammatory drugs helps in long-term maintenance, while short-term administration of steroids or antifibrotic drugs aids in transiently inhibiting initial immune cell engagement.[2,5] However, these anti-inflammatory drugs, administered systemically or locally, have multiple targets and can lead to differential non-specific effects and associated toxicity in vivo.[6] Similarly, the widespread use of antibiotics to prevent implant-associated infections has raised concerns relating to multidrug resistance and the evolution of superbugs, which has inspired the study into non-antibiotic-based therapy for infection management.[7,8]

Alternatively, surface modifications to silicone-based biomaterials have recently been the focus to prevent implant-associated fibrosis and infection. It is the surface of the biomaterial that dictates its fate. Hence, surface functionalization methods such as antimicrobial peptides grafting,[9] bioactive polymers (zwitterionic polymers -poly(2-methacryloyloxyethyl phosphorylcholine);[10,11] low fouling hydrophilic polymers – poly(ethylene glycol), poly(ethylene oxide),[12]) and use of proteins (human serum albumin,[13] itaconic acid conjugated gelatin)[14] have been employed to curtail implant-associated complications. Though these strategies have been proven to prevent either fibrosis or infection independently (Table S1, electronic Supporting Information), concomitant prevention of fibrosis and infection has remained elusive. Multi-compartment nanocomposite systems have shown promise, wherein core–shell electrospun matrices releasing an antibiotic (ampicillin) and an immunomodulatory factor [a nuclear factor-κB (NF-κB) inhibitor – Bay11–7082][15] have been investigated but not on silicone-based biomaterials. Nitric oxide (NO) releasing polymer coatings have been previously reported to reduce fibrous capsule thickness by 50%,[16] and NO-releasing silicone-based substrates have shown antibacterial efficacy while reducing foreign body response.[17]

NO is a potent gasotransmitter with multiple physiological roles such as regulating vascular physiology (vasodilation, antithrombotic), modulating immune response, neurotransmission, facilitating remodeling (proangiogenic and wound healing), and generating oxygen-independent free radicals.[18] NO is also a proven bactericidal agent that adopts multiple mechanisms to exhibit its antimicrobial properties, including nitrosation of amines and thiols of bacterial proteins, lipid peroxidation, and chemical damage to nucleic acids.[19] It is because of this multi-pronged approach that bacteria cannot develop resistance to NO, making it a superior candidate to conventional antibiotics. NO-releasing substrates have been investigated previously (Table S1, Electronic Supporting Information), but in the current work, the feasibility of developing a NO-generating interface, harnessing the S-nitrosothiols (RSNOs) as NO donor has been investigated. Endogenous RSNOs such as low molecular weight S-nitrosoglutathione (GSNO) are ubiquitously present in the body at concentrations 0.02–1 µM in human blood,[20] 300 nM–4 µM in human bronchoalveolar lavage fluid[21] and ≈0.09 µM in subcutaneous tissue level.[22] This endogenous reservoir of NO can be harnessed if a catalytic interface is developed on a biomaterial surface, which can lead to a localized (in situ) NO generation, thereby facilitating multiple therapeutic outcomes at the implant site. RSNOs are catalyzed by metal ions to generate NO, with Cu^{+} being the most widely studied metal ion catalysis.[23,24]

Bioactive glasses, particularly mesoporous bioactive glasses obtained through sol–gel synthesis, offer the advantage of doping the SiO_2 network formers with other network modifiers of other metal oxides such as calcium oxide (CaO), Phosphorus pentoxide (P_2O_5), copper (II) oxide (CuO), and strontium oxide (SrO), which attribute multifunctional traits to the chosen glass composition.[25] Herein, the role of copper and strontium as metal catalysts for RSNO decomposition is investigated with a well-reported 70S bioactive network ($70SiO_2.25CaO.5P_2O_5$)[26] which was doped with either copper ($70SiO_2.20CaO.5CuO.5P_2O_5$) or strontium ($70SiO_2.20CaO.5SrO.5P_2O_5$)[23] to synthesize mesoporous nano-bioactive glass particles. An in situ NO generating (NOgen) interface was developed by incorporating the synthesized particles with room temperature vulcanizing (RTV) silicone elastomer and coating them onto silicone substrates via a dip coating technique. The modified substrates with NOgen capabilities were then holistically investigated in vitro for their potency: i) to generate NO from physiologically relevant levels of endogenous NO donor (GSNO); ii) thus generated NO was investigated for its antibacterial, antithrombotic effects and cell-instructive roles on human fibroblasts, endothelial cells, and macrophages. Additionally, we also investigated the effect of strontium ions released from the NOgen interface in regulating cellular activity pertaining to fibroblast migration and macrophage activation.

2. Results and Discussion

2.1. Doping Bivalent Metal Ions in Mesoporous 70S Bioactive Glass for Nitric Oxide Generation

A 70S bioactive glass ternary network was chosen here, owing to its better bioactivity, higher density of Si-OH exposed groups (ideal for bonding when coating), and enhanced glass dissolution traits[27] (in comparison to well-characterized 45S5 melt-derived bioactive glasses), making it a resorbable bioceramic without eliciting any adverse immune response. To obtain the sol–gel derived nano-bioactive glass particles, a modified Stöber's method with the sacrificial template of hexadecyltrimethylammonium bromide (CTAB) was used. As a surfactant, CTAB helps in templating and serves as a capping agent to control the size of the synthesized particles. Moreover, when the templating agent is removed, it obtains a mesoporous network (**Figure 1A**), which has shown immense potential in drug delivery applications owing to its large specific area, low density, and good penetration capability.[28] These properties are desired in a nanoparticle system that is intended to be used as an in situ nitric oxide nanogenerator, where NO donor should be able to access the catalytic site and decompose easily. The current work investigated the potency of two metal ions: copper and strontium for the catalytic sites. These metals were introduced as oxides that acted as network modifiers within the tetrahedra silicate network, which was connected by —Si—O—Si— bridging oxygen bonds. Thus, the bioactive glass particles obtained from 70S bioactive glass: $70SiO_2.25CaO.5P_2O_5$ were termed **nBG**, copper doped network:

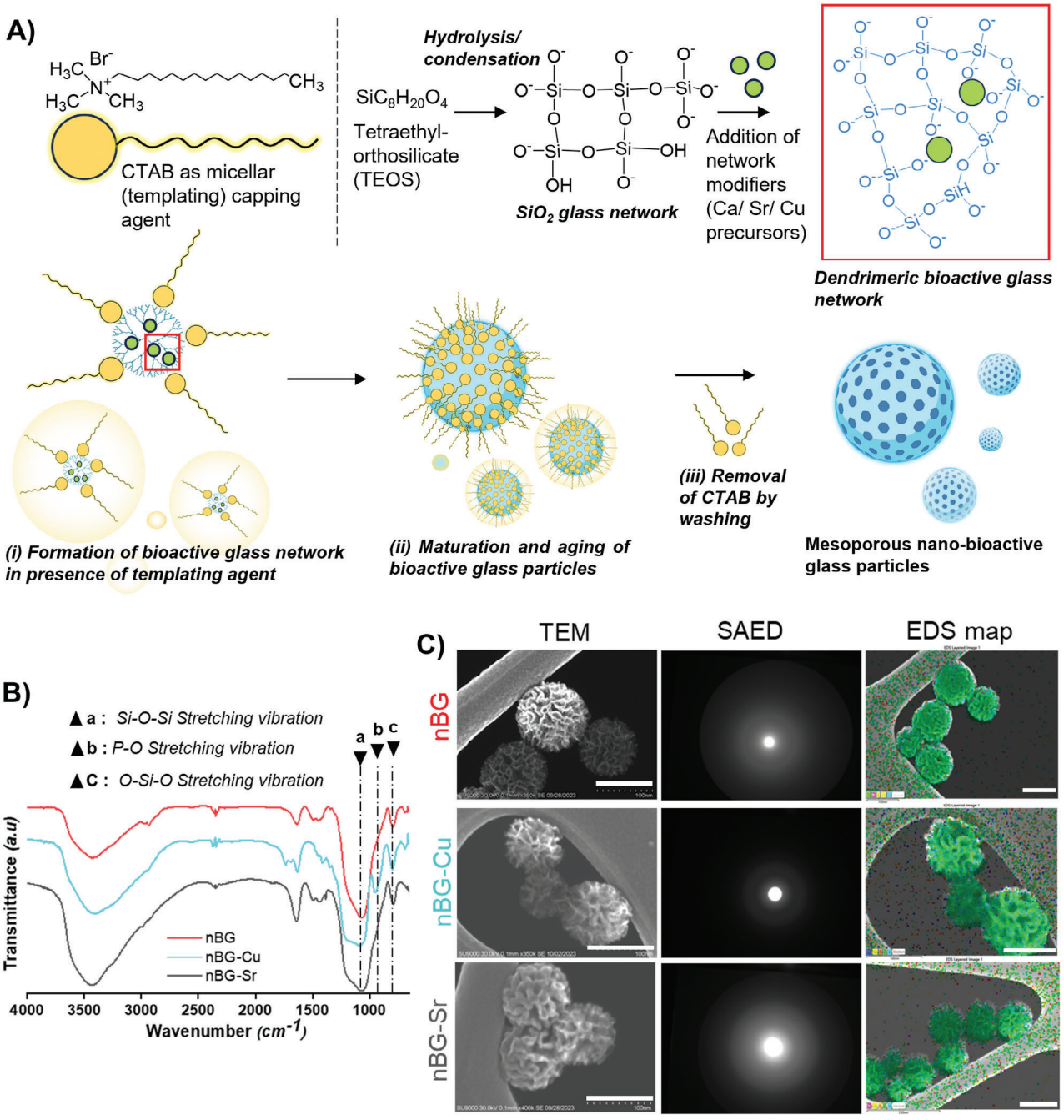

Figure 1. Synthesis and characterization of mesoporous nanobioactive glass nitric oxide generating particles. A) hexadecyltrimethylammonium bromide (CTAB) assisted sacrificial templating synthesis of nanobioactive glass by modified Stöber's method; B) Fourier transform infrared spectra of synthesized nano-bioactive glass (nBG), copper doped BG (nBG-Cu), strontium doped BG (nBG-Sr); C) Transmission electron microscopy (TEM) analysis of synthesized nanoparticles showing dendrimer-like nature of glass network; selected area energy diffraction (SAED) showing amorphous nature of the nano-bioactive glasses and energy dispersal spectral (EDS) mapping of particles confirming stoichiometry of the glass composition (scale bars represented are 100 nm).

$70SiO_2.20CaO.5CuO.5P_2O_5$ as **nBG-Cu**, and strontium doped network: $70SiO_2.20CaO.5SrO.5P_2O_5$ as **nBG-Sr**. Both copper and strontium are bivalent cations that exhibit +1 and +2 oxidation states and are predominantly present in their +2 oxidation state within the glass network in its oxide form. Though copper has been well validated in its role in catalyzing S-nitrosothiols,[20] this is the first report investigating the catalytic potency of strontium. Moreover, strontium has been reported to possess other ancillary benefits in regulating cellular fate involving neuronal plasticity, angiogenesis, and osteoclast activity.[29,30] Infrared spectra of the synthesized nBG, nBG-Cu, and nBG-Sr confirmed the fingerprint regions of the bioactive glass network (Figure 1B). The

stretching vibration of Si—O—Si at 1093 cm^{-1} (as a shoulder peak) and stretching vibration of O—Si—O at 800 cm^{-1} from the SiO_2 network formers; the P—O bending vibration at 962 cm^{-1} from P_2O_5 network modifiers[26] were noticed in all the sample types.

Previously, it has been reported that the concentration of the surfactant dictates the templating characteristics and order of the mesoporous network. For instance, when 0.4 mM CTAB was used, it resulted in a particle size of ≈150 nm, whereas 10 mM resulted in ≈100 nm particles.[31] Similarly, anything below 3 mM CTAB had a specific area of ≈444 m^2 g^{-1}, while above 6 mM had a specific area of ≈970 m^2 g^{-1}. For this system, an optimal concentration of CTAB for the balance of the correct particle size and the specific area was found to be 4 mM, which yielded nanoparticles of the order ≈100 nm (Figure 1C). Monodispersed spherical nano-bioactive glass particles with dendrimer-like projections arising from maturation of the bioactive glass network were obtained (as observed from the TEM), while no difference in size was noted between the groups (nBG, nBG-Cu, and nBG-Sr). Moreover, warm ethanol refluxing[26] was used to remove the templating agent to create the mesopores (instead of calcination), which resulted in nanoparticles having an amorphous nature as observed by the diffused rings from selected area energy diffraction (SAED) patterns (Figure 1C). The energy dispersal spectral (EDS) confirmed the stoichiometric composition of the synthesized glass network where the incorporation of Cu (in nBG-Cu), Sr (in nBG-Sr), calcium (Ca), and phosphate (P) as network modifiers were mapped and found to be distributed throughout the network former Si (in SiO2) (Figure 1C; Figure S2, electronic Supporting Information). The hydrodynamic radii of nanoparticles were analyzed (dispersant: ethanol, viscosity = 1.0740 cP and refractive index = 1.361) (Figure S3A–C, electronic Supporting Information) and the average diameter (polydispersity index – PDI, Zeta potential – ζ, in parenthesis) in suspension for nBG was 358 ± 181 nm (PDI = 0.181; ζ = 13.6 mV), nBG-Cu was 222 ± 77 nm (PDI = 0.295; ζ = 12.8 mV), and nBG-Sr was 280 ± 107 nm (PDI = 0.221; ζ = 13.2 mV). No difference was noted between the hydrodynamic radii and the zeta potential of the analyzed samples, and the values were in agreement with the nano-bioactive glass systems previously reported.[26] The network modifiers used here did not impact the microstructure or its property in suspension. The suspensions were stable in ethanol after 4 h (Figure S3D, electronic Supporting Information), indicating that they are suitable for dip coating application when incorporated in a polymer solution.

2.2. Facile Modification of Silicone Substrates to Obtain NOgen Interface by Dip Coating

NO is one of the classical gasotransmitters (the other two being hydrogen sulfide and carbon monoxide) that regulates key cellular signaling cascades of vascular, neural, and immune homeostasis. NO is generated by endothelium with an estimated flux 0.5 to 4 × 10^{-10} mol cm^{-2} min^{-1}[32] as a product of oxidation of L-arginine into L-citruline mediated by enzyme (endothelial nitric oxide synthase – eNOS) in the presence of molecular oxygen and reduced NADPH (nicotinamide adenine dinucleotide phosphate) as co-substrates. In addition to eNOS, neuronal NOS (nNOS) and inducible NOS (iNOS) expressed by cells of neuronal lineage and immune cells (respectively) can also facilitate the production of NO in vivo. The gasotransmitter is short-lived, and it exerts its cellular signaling by activating a key secondary signaling messenger – soluble guanylate cyclase (sGC), which activates the NO/sGC/cGMP (cyclic guanosine monophosphate) signaling axis.[33] NO generated by these cells also exerts another important role, which is S-nitrosylation of thiol groups of L-cysteine of proteins generating S-nitrosothiols (such as S-nitrosoalbumin or S-nitrosoglutathione – GSNO) which are generally present in the human body and are the major sources of NO donors that can be harnessed to generate NO in an enzyme and cell-independent fashion.

To produce a localized NO flux at a biomaterial implant site to harness the cell instructive facets of NO, a NOgen interface needs to be developed on the biomaterial. The NOgen interface can utilize the NO donors present in the vicinity to catalyze its decomposition and generate NO in situ. This was achieved in a facile manner by dip-coating SR substrates with different concentrations (5, 15, 25, and 50 mg mL^{-1} suspensions) of synthesized nanobioactive glasses in RTV silicone elastomer polymer to obtain conformal coatings which are cured at ambient temperatures (**Figure** 2A,B). Anything above 50 mg mL^{-1} concentration led to delamination of the coating, and concentrations in 5 and 15 mg mL^{-1} resulted in non-homogenous or patchy coatings. The modified substrates were analyzed for the NO generation capability (Figure 2C) using a chemiluminescence-based real-time NO analyzer to determine the flux values in the monitored 30 min duration (Figure 2D, at 37 °C, in phosphate-buffered saline PBS, pH 7.4 supplemented with 1 and 30 µM GSNO and reduced glutathione – GSH respectively, akin to the physiological levels of GSNO and GSH in blood[20,34] reported earlier). S-nitrosothiols (like GSNO) can be decomposed to release NO through photolytic, thermal, and metal ion-assisted mechanisms. Among these, metal-ion-mediated catalysis was of interest to us here since copper (Cu^{2+}/ Cu^{+1}) has long been proven and extensively used as an effective reagent for GSNO catalysis.[35]

A gamut of bivalent metal ions such as Zn, Ca, Mg, Ni, Co, Mn, Cr, Pd, Pt, and trivalent Fe, Au, and V have been investigated for their potency to catalyze GSNO decomposition.[24,36] Among which, Cu^{2+}, Au^{3+}, Pd^{2+}, Pt^{2+} and V^{3+} were demonstrated to be the most potent metal-ion catalysts. Copper has been an important biological metal ion used as a cofactor in several metalloenzymes. Here, the efficacy of another important bivalent metal ion, Sr, as a catalyst was explored. For this purpose, the bioactive glass network was doped with oxides of Cu (a known metal ion catalyst) and Sr, which has several ancillary cell instructive benefits, to investigate the doped-nano bioactive glass systems to catalyze GSNO decomposition. A concentration-dependent increase in total moles of NO generated from nBG-Cu and nBG-Sr groups was observed with a saturation point at 50 mg mL^{-1} concentrations dip coats (Figure 2C). The total moles of NO released from nBG-Cu 50 and nBG-Cu 25 were found to be 3.6 ± 1.12 and 3.58 ± 0.52 nmol whereas nBG-Sr 50 and nBG-Sr 25 released 2.96 ± 0.85 and 2.45 ± 0.48 nmol of NO, respectively. As expected, the control nBG group did not aid in GSNO catalysis as the molecular constituents Si, P, or Ca have not been shown to participate in NO generation[36] (Figure 2Diii). The doped nanobioactive glass was able to generate NO at reduced GSNO and GSH concentrations as noted in other tissue spaces, such as

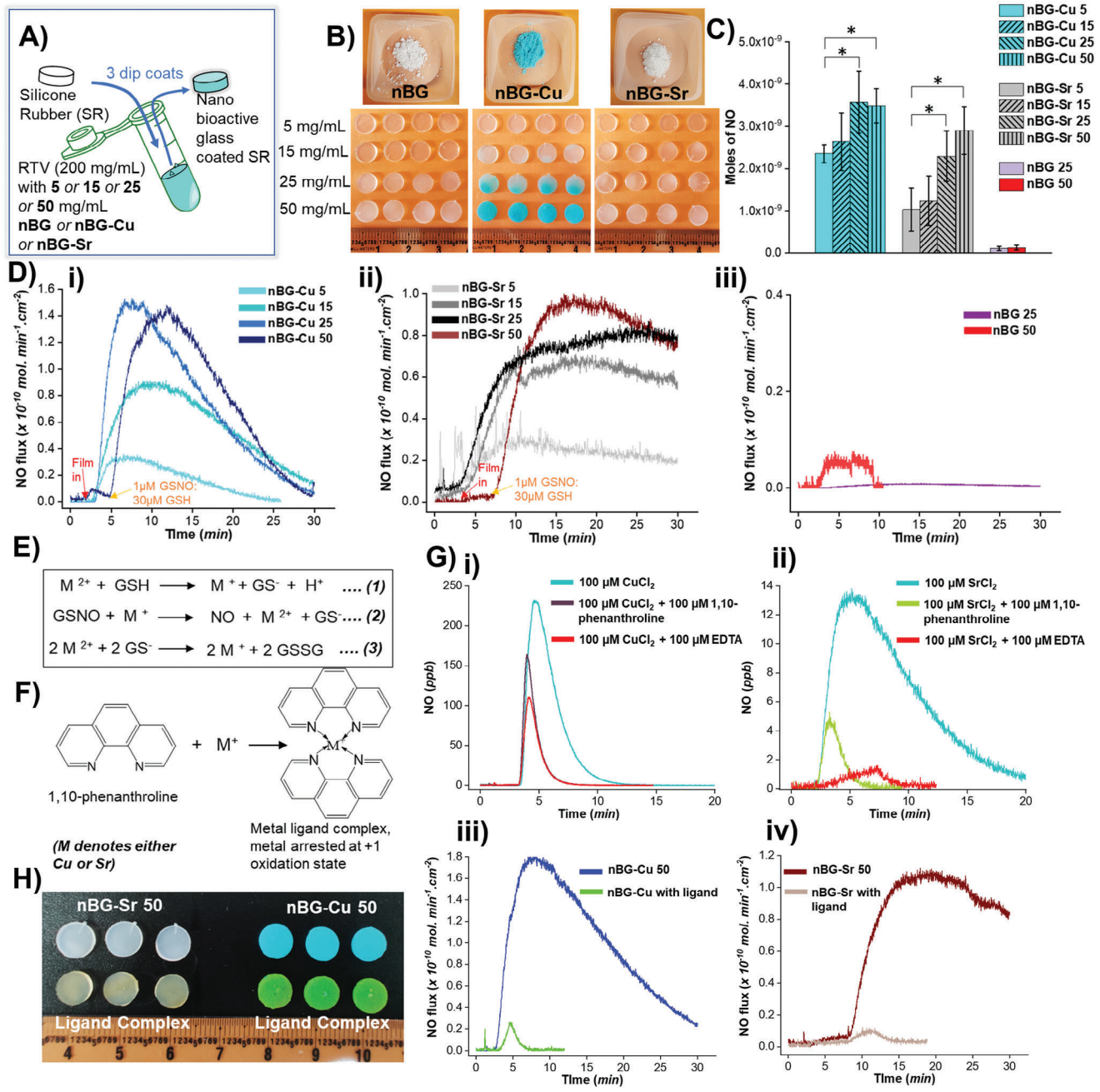

Figure 2. Facile modification of silicone rubber (SR) substrates by dip coating method to develop a nitric oxide generating (NOgen) interface. A) dip coating of SR substrates with different concentration of nanobioactive glasses with room temperature curing silicone (RTV) and B) the resultant gross morphological appearance of coated substrates; C) chemiluminescence nitric oxide analysis of coated substrates (total moles of NO generated per 1 μM GSNO/ 30 μM GSH injection) and D) its representative NO generation curve for different concentrations of i) nBG-Cu, ii) nBG-Sr, and iii) nBG; E) Reaction scheme summarizing the mechanism and regeneration of metal ion assisted nitric oxide generation from the NOgen interface; F) Understanding the mechanism of decomposition of GSNO by metal ion (+1 oxidation state) by arresting it with a ligand (1,10- phenanthroline); G) chemiluminescence nitric oxide analysis of decomposition of 1 μM GSNO (with 30 μM GSH) in i) presence of copper or ii) strontium salts and chelating agents ethylenediaminetetraacetic acid (EDTA) or 1,10 phenanthroline; and with NOgen films: iii) nBG-Cu 50, iv) nBG-Sr 50; H) color change post incubation with ligand (1,10 phenanthroline) indicative of metal (+1 oxidation state)-ligand complexation formation, and the arrest of NO generation. [Data are presented as means ± S.D; ($n \geq 4$) for nitric oxide analysis); Parametric ANOVA, Tukey's post hoc test was performed; * indicates significance at $p \leq 0.05$].

in human bronchoalveolar lavage fluid (300 nM–4 μM)[21] and in subcutaneous tissue level (≈0.09 μM) as well.[22] It was also found that the total moles of NO also reduced corresponding to the GSNO supplemented with: i) 0.3 μM GSNO, total moles released for nBG-Cu 50 was 2.1 ± 0.41 nmol, nBG-Cu 25 was 1.22 ± 0.73 nmol; for nBG-Sr 50 was 1 ± 0.66 nmol, nBG-Sr 25 was 0.58 ± 0.08 nmol; ii) 0.09 μM GSNO, total moles released from nBG-Cu 50 was 0.48 ± 0.05 nmol, nBG-Cu 25 was 0.16 ± 0.07 nmol; from nBG-Sr 50 was 0.09 ± 0.006 nmol, nBG-Sr 25 was 0.05 ± 0.009 nmol. (Figure S4, Electronic Supporting Information).

The mechanism for the metal ion mediated catalysis was further studied by performing the decomposition of 1 μM GSNO (with 30 μM GSH) in presence of two types of metal chelators: i) ethylenediaminetetraacetic acid (EDTA) which has specificity for +2 valency state of metal ions, and ii) 1,10 phenanthroline which has specificity for +1 valency state of metal ions of copper and strontium.[36,37] It is regarded that the metal (M) ion used here exists in its +2 valency (M^{2+}), which gets reduced by a reducing agent like glutathione (GSH), to yield a reduced form of M^{+} ion which catalyzes the GSNO decomposition to release NO and thereafter regenerating the M^{2+} ion which participates in the catalysis again[36] (Figure 2E). Computational modeling has revealed that GSNO coordinates with the M^{+} metal ion center via its sulfur, and once NO is released, glutathione disassociates from the complex.[35] To test this hypothesis for a bivalent cation such as Sr, the active catalytic center M^{+} was arrested with 1,10 phenanthroline ligand (Figure 2F). Chemiluminescence NO analysis corroborated this, where in the presence of 100 μM of either metal ion salt: copper chloride (Figure 2Gi), or strontium chloride (Figure 2Gii), the NO catalysis which typically occurred was arrested instantaneously in the presence of EDTA while NO catalysis was retarded to a significant extent in the presence of 1,10-phenanthroline. UV–vis spectroscopic analysis of metal ion and 100 μM ligand (1,10 phenanthroline) interaction revealed that in the absence of a reducing agent (GSH), +1 valency state was not achieved; whereas in the presence of the reducing agent +1 valency state was obtained and $(\text{metal-ligand})^{+1}$ complex (having an absorption peak at λ_{max} = 450 nm) was formed (Figure S5, electronic Supporting Information). When the NOgen efficacy of nBG-Cu 50 and nBG-Sr films was tested in the presence of the 1,10 phenanthroline ligand, the NO catalysis was arrested significantly (Figure 2Giii–iv). Interestingly, when the films (NOgen substrates) were retrieved from the NO analysis chamber, there was a color change (Figure 2H); white strontium films turned reddish brown, whereas copper films changed color from teal to green. This is indicative of the $(\text{metal-ligand})^{+1}$ complex having a reddish brown-colored product formation with an absorption peak at λ_{max} = 450 nm.[36]

Kinetic analysis on rate forms of metal ion-mediated GSNO decomposition has shown to have first-order dependencies (upon both concentration levels of GSNO and copper).[35,38] The reaction rate constants (k) can be determined from NO flux profiles (Figure 2Di–ii) by plotting time (t) versus ln ($[GSNO]_t$ /$[GSNO]_{t=0}$), yielding a linear equation ($y = mx$), where the slope gives the rate constant ($k = \frac{d[NO]}{dt} = -\frac{-d[GSNO]}{dt}$; for equation (2) in Figure 2E). The rate constant for nBG-Cu 50 was found to be 8.65×10^{-3} and 3.67×10^{-3} s^{-1} in the presence of 1 μM GSNO (as NO donor), that is, k of Cu mediated $\frac{-d[GSNO]}{dt} > k$ of Sr mediated $\frac{-d[GSNO]}{dt}$; which explains why Cu is a more potent catalyst in comparison to Sr. The rate constant for only nBG 50 films (Figure 2Diii) was found to be 2×10^{-5} s^{-1} which served as the control group where no metal-assisted catalysis of NO donor took place. The average flux values generated for 1 μM GSNO supplementation from nBG-Cu 50 was 1.72×10^{-10} mol cm^{-2} $min^{-1,}$ and from nBG-Sr 50 was 1.12×10^{-10} mol cm^{-2} min^{-1} which was in the physiologically relevant levels seen in the endothelium.[32]

2.3. Multifunctional NOgen Interface Exhibits Antibacterial and Antithrombogenic Properties

Several active and passive surfaces or interfaces have been developed on SR substrates to combat implant-associated thrombosis (occurs within minutes to hours) and early onsite infection (initiated within hours to days). Of particular interest are the interfaces that modulate the wettability of the surfaces to obtain either super-hydrophilic or super-hydrophobic surfaces (Table S1, electronic Supporting Information lists a few of these attempts[39–41]). These passive strategies prevent protein-fouling and cell (bacterial and mammalian) adhesion. However, these methods are generally regarded as advantageous for short-term applications as these coatings are not that durable in vivo and require the use of complex chemistry. Liquid or lubricant infusion to make SR substrates slippery also faces drawbacks due to the leaching or deswelling of these infused liquids, rendering these antifouling surfaces ineffective. Pertinent to note here, the approach of introducing nano-bioactive glass by dip coating the SR substrates did not alter the surface wettability much, as a modest increase in static water contact angle was seen with increasing nanoparticle concentration in comparison to SR control (Figure S6, Electronic Supporting Information). Similarly, the water uptake percentage of SR control was found to be 0.5 ± 0.24 wt.%, which was not significantly different for the modified substrates (nBG-50, nBG-Cu, and nBG-Sr was found to be 0.49 ± 0.14 wt.%, 0.53 ± 0.2 wt.% and 0.51 ± 0.16 wt.% respectively). NO-releasing materials have effectively curtailed microbial growth and colonization on NO donor-incorporated silicone-based devices (Table S1, electronic Supporting Information).[17,42] Here, the efficacy of physiologically relevant levels of NO generated from NOgen substrates when challenged against planktonic cultures of two commonly noted bacterial strains associated with implant infections: Gram-negative *Escherichia coli (E. coli)* and Gram-positive *Staphylococcus aureus (S. aureus)* were tested (**Figure 3A**). The NOgen substrates were effective in reducing the viability of *S. aureus* by ≈1.1 log (p = 0.0056) for nBG-Cu 50 (≈92% bacterial reduction), ≈0.4 log (p = 0.032) for nBG-Cu 25 (≈70% bacterial reduction); while ≈1 log (p = 0.0066) for nBG-Sr 50 (≈90% bacterial reduction), and only ≈0.2 log (p = 0.037) for nBG-Sr 25 (≈55% bacterial reduction) in comparison to SR controls and nBG groups. In the case of *E.* coli, ≈1.4 log reduction (p = 0.0052) for nBG-Cu 50 (≈93.3% bacterial reduction) and ≈1.2 log reduction (p = 0.0064) (≈93% bacterial reduction) for nBG-Sr 50 were observed. Since the NO levels generated here were in the physiological range, they are expected to have a bactericidal effect while not imposing excessive nitrosative or oxidative stress

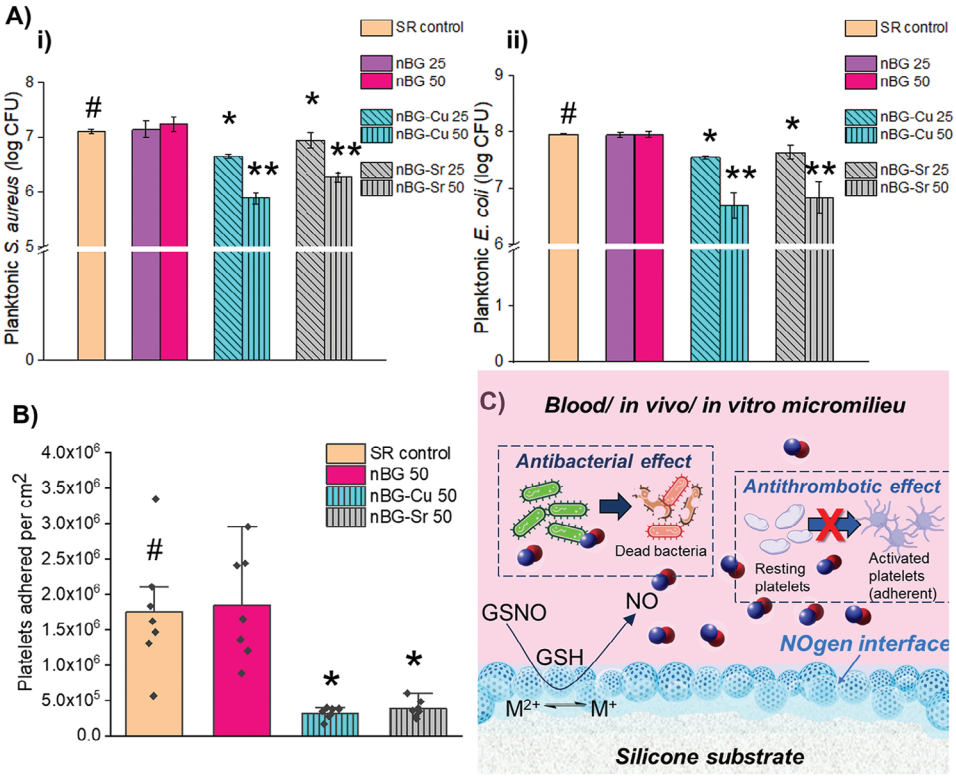

Figure 3. Multifunctional NOgen interface on SR substrates bestows antibacterial and antithrombotic attributes. A) antibacterial activity of NOgen and SR control substrates assessed by challenging against planktonic cultures of two commonly noted bacterial strains associated with implant infections: i) Gram-negative, Escherichia coli and ii) Gram-positive Staphylococcus aureus; in the presence of 1 μM GSNO/ 30 μM GSH supplementation every hour for 4 h; B) antithrombotic effect of NOgen substrates tested by exposing porcine-derived platelets to these substrates for 90 min in presence of 1 μM GSNO/ 30 μM GSH supplementation; C) illustration depicting the metal ion-assisted NO generation from NOgen interface holding promise in reducing implant associated infection and reducing platelet activation (thrombus formation). [Data are presented as means ± S.D; (($n \geq 4$) for antibacterial study; ($n \geq 6$) for platelet adhesion study); Parametric ANOVA, Tukey's post hoc test was performed; * indicates significance at $p \leq 0.05$ and ** indicates significance at $p \leq 0.01$, in comparison to # SR control].

on mammalian cells.[43] Furthermore, the hallmark antithrombotic effect of NO (for only 50 mg mL^{-1} groups, since it had better antibacterial efficacy) was tested by checking the extent of activated platelets adhered to SR control and NOgen substrates (Figure 3B). Both the NOgen surfaces exhibited a drastic reduction in adhered platelets: 81.5 ± 3.6% reduction for nBG-Cu 50, and 77.5 ± 2.4% reduction for nBG-Sr 50 group in comparison to SR control, showcasing the NOgen's potency to inhibit activated platelet adhesion. This result agrees with a prior study that showed that NOrel material significantly reduced platelet adhesion to SR surface while substrate coated with anticoagulant heparin exhibited non-significant reduction.[44] The developed in situ NOgen interface (Figure 3C), which could generate NO from endogenous RSNOs, can help mitigate implant-associated early onsite infection in medical devices and can also be effective in preventing implant-associated thrombosis for direct-blood contacting devices. The mechanism of NO to elicit antibacterial action relies on the nitrosation of amines and thiols of bacterial proteins, lipid peroxidation, and chemical damage to nucleic acids;[19] while inhibition of platelet activation relies on activation of NO/sGC/cGMP signaling axis which downregulates the activity of a key cell-adhesion receptor ($\alpha II_b\beta_3$ integrin) present in platelets.[32,33]

Active strategies rely on the release of an antimicrobial, antifibrotic, or anti-thrombotic agent or even dual/multi-release systems. However, the bioactivity and undesired action of released cargo always pose a risk in regulatory clearance for clinical translation prospects. The 70S bioactive glass used here belongs to an amorphous resorbable glass network where the glass dissolution occurs at physiological conditions. The leaching of metal ions from the SR control and modified NOgen substrates at different time points was tested by incubating the films in phosphate-buffered saline (pH 7.4) at 37 °C (Figure S7A–C, Electronic Supporting Information). The network formers (SiO_2) in the form of Si ion concentration were found to be in the range of 80 to 150 μg g^{-1} of the sample (cumulative release at day 14), which is in the cytocompatible range of 160 ppm[45] to regulate cellular fate monocyte-macrophage cell line, J774.2 (in vitro) and below the lethal dosage (LD_{50} = 2000 mg kg^{-1}) for colloidal silica in rat models.[46] The Cu ion concentration leaching noted in nBG-Cu 50 at day-14 was ≈66 μg g^{-1} of the sample, which was also on par with the tolerance levels above which the initial hepatotoxic effects are noted in rats.[47] The Sr ion concentration in leachates from nBG-Sr at day-14 was ≈40 μg g^{-1} of sample and is within the therapeutic dosage < 300 mg k^{-1} g administered to have beneficial effects in osteoporotic rodents.[48] Therefore, the current

system was not only successfully able to generate and relatively sustain the NO generation at physiologically relevant levels for 21 days (Figure S8, Electronic Supporting Information), but was also capable of releasing therapeutic ions (such as Cu or Sr) at levels which could have cell-instructive effects at the implant site. Calcium sensing receptors (CaSRs) and other G-protein coupled receptors (GPCR 6A) have an affinity for such bivalent cations, which mediate the downstream activity upon activation by these cations. These CaSRs are constitutively expressed in fibroblasts and macrophages and can impact their cellular fate.[49]

2.4. NOgen Interface and the Cell-Instructive Effect of Strontium on Fibroblasts

The foreign body response is a multi-staged process involving multiple cells (macrophages, neutrophils, and lymphocytes) in the implant vicinity (Figure S1, Electronic Supporting Information). Macrophage trafficking and fibroblast activation are two crucial events determining the extent of the inflammation and fibrous encapsulation, thereby dictating the fate of the implanted biomaterial.[12] To prove the coatings used here to develop the NOgen interface are cytocompatible, a cytocompatibility assessment using human fibroblasts was performed following ISO standard (ISO10993-5: 2009) protocol by i) exposing the leachates on fibroblasts and ii) through contact method using transwell inserts which are followed for testing biomedical devices safety in vitro for implantable devices (**Figure 4A**). All the tested groups (nBG, nBG-Cu, and nBG-Sr; 25 and 50 mg mL^{-1} dip coat variants) exhibited a percentage cellular viability index greater than the 70% tolerance threshold regarded as safe for use in implantable silicone-based medical devices.[50] Though no discernible difference between test groups and cell control was noted in the contact method (Figure 4Aii), the leachates (Day-7 and Day-14) of the treated cells showed a decreased viability index. The assay used relies on the reduction of MTT (3-[4,5-dimethylthiazol-2-yl]-2,5 diphenyl tetrazolium bromide) by mitochondrial dehydrogenase enzyme to form purple formazan crystals, which correlate to the viability. However, when cells are exposed to certain compounds or cargoes, the bioenergetics could be altered; the cells remain viable, but the mitochondrial activity is slightly reduced.[51,52]

This hypothesis was further investigated by testing the efficacy of leachates (day-14) against activated fibroblasts. One of the pivotal events in implant-associated fibrosis is the recruitment and activation of fibroblasts in response to inflammatory triggers. This, alongside other signaling mechanisms, differentiates into myofibroblasts, which secrete excessive collagenous matrix.[12] To activate the fibroblasts, a known stimulant, ascorbic acid (AA) enters the cells via sodium-dependent vitamin C (SVCT 1 or 2) transporters and upregulates the collagen gene expression levels.[53] This is evident with the approximately five-fold increase in collagen secretion noted in AA-treated fibroblasts compared to untreated control (Figure 4B,C). To these activated fibroblasts, the nBG-Cu 50 and nBG-Sr 50 leachate treatment had a considerable reduction in collagen secretion (≈1.5-fold reduction for nBG-Cu and approximately 5-fold reduction in comparison to AA-treated controls). The migration potency of activated fibroblasts and the effect of leachates was evaluated by an *in vitro* wound closure assay (Figure 4D,E). Overlapping with excessive extracellular matrix (ECM) production is the migration of protofibroblasts into these provisional ECM, which later get activated into myofibroblasts.[4] Hence, the recruitment of fibroblasts at the implant site becomes an essential step in peri-implant fibrosis, and if any active surface can retard this, it could be beneficial. The nBG-Sr 50 leachate-treated groups significantly reduced the migration of these activated fibroblasts (≈1.66-fold reduction in comparison to AA-treated cell control).

One of the key regulators of collagen gene expression is the speckled protein (Sp) family, where Sp 1 and Sp 3 transcription factors bind upstream to the *collagen-α1* gene and upregulate its expression.[54] The molecular mechanism for increased collagen expression in AA-treated fibroblasts is due to the increased levels of malondialdehyde noticed in the cytosol, which positively influences the expression of Sp1 and Sp3 proteins, thereby upregulating collagen expression.[53] Strategies that involve modifying biomedical surfaces, such as Ti surfaces with flavonoids (anti-inflammatory: quercetin or taxifolin),[55] drastically reduce fibroblast activity. This is because anti-inflammatory drugs target the inflammatory (particularly cyclooxygenase-2 COX-2 dependent) cascade which shares a common nexus with Sp 1 and Sp 3 expression.[56] In this investigation, 14-day leachates which had Sr concentration (≈16 µM) had a therapeutic outcome downregulating collagen expression and retarding the fibroblast migration. Low doses of trace metal ions such as Mg, Se, and Sr have been found to downregulate COX-2 activity thereby having anti-inflammatory potential.[29,30] Moreover, strontium ranelate (Sr^{2+}) has also been reported to downregulate the transforming growth factor TGF-β1/NFκB (nuclear factor κ B) signaling axis,[57] which is one of the predominant pathways targeted by multiple antifibrotic drug-releasing platforms to combat capsular contracture[2] and treating fibrosis.[58]

2.5. Effect of Copper and Strontium from Leachates of NOgen Interface on Macrophages

To test the anti-inflammatory effect of Sr, the leachates were tested on naïve human macrophages, and the polarization fate of macrophages was assessed (**Figure 5**). For this, as a reference population, inflammatory cytokine (interferon INF-γ) treated macrophages (now polarized into M_1 phenotype), and similarly anti-inflammatory cytokine (interleukin IL-4) treated macrophages (now polarized into M_2 phenotype) were used (Figure S9, Electronic Supporting Information). These M_1 and M_2 populations had distinct morphological appearances: M_0 macrophages were more rounded, M_1 macrophages were filamentous and star-shaped, and M_2 had a more spread-out nature (Figure S9, Electronic Supporting Information). The population was characterized quantitatively by flow-cytometry and qualitatively visualized using immunostaining by probing for cell surface markers: CD 68 (pan macrophage marker), CCR7 (inflammatory marker present in M_1) and CD 206 (anti-inflammatory marker M_2 macrophages) (Figure S10, Electronic Supporting Information). As expected, INF-γ treated naïve macrophages predominantly expressed CCR7 while IL-4 treated naïve macrophages predominantly expressed CD 206; as INF-γ would induce them into M_1 phenotype (having low M2/M1

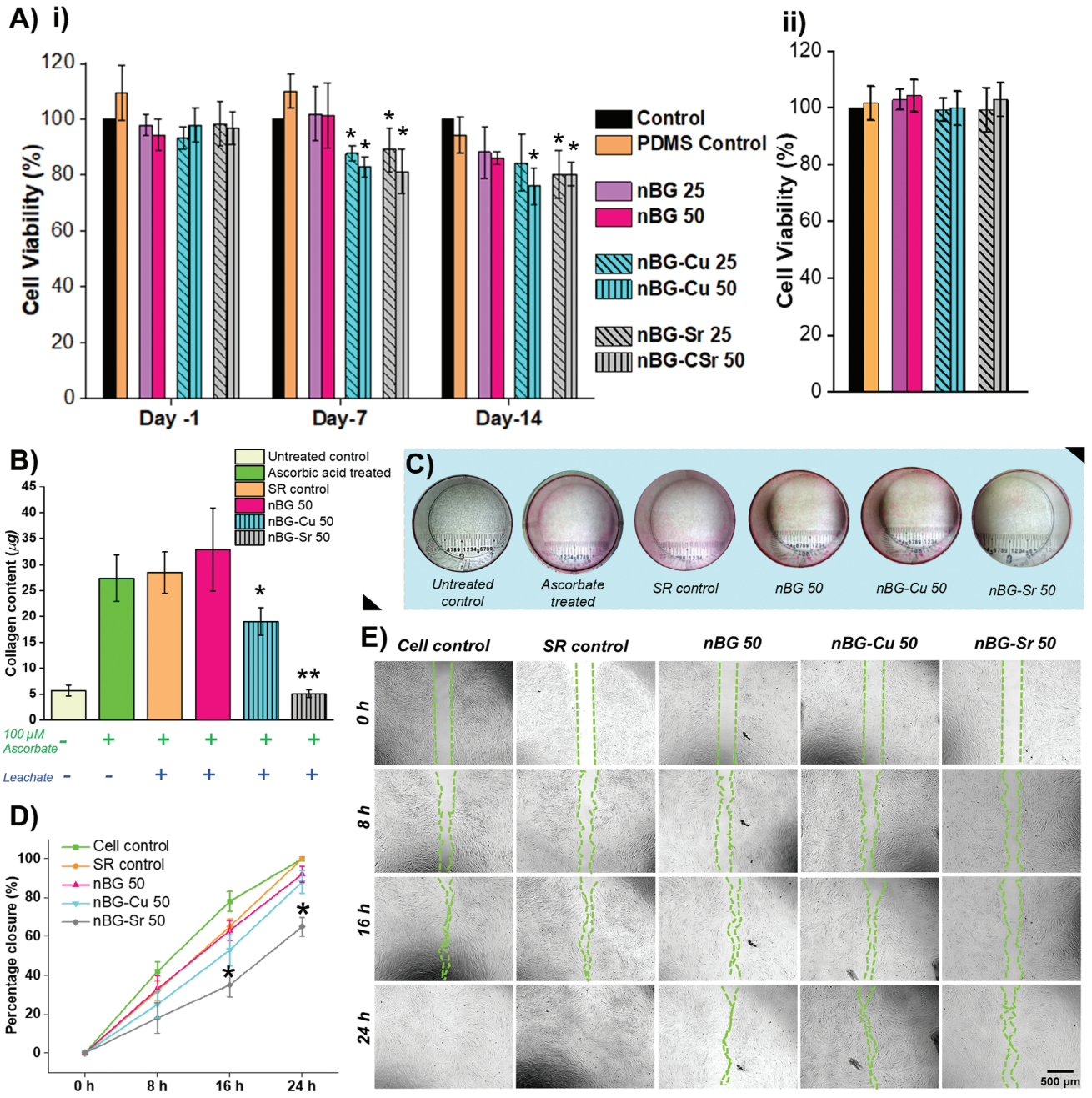

Figure 4. Cytocompatibility and in vitro fibrosis assay on NOgen interface and its leachates. A) Cytocompatibility assessment using human fibroblasts by following ISO standard (ISO10993-5: 2009) protocol by i) collecting leachates and ii) through indirect contact method. Ascorbic acid-induced upregulation of fibroblast activity and the effect of leachate on its downregulation (by nBG-Sr 50) tested by: B) collagen estimation by Sirius red assay and C) representative well images showing red coloration of collagen deposits; D) fibroblast migration assessed by in vitro wound closure and E) representative phase-contrast micrographs. [Data are presented as means ± S.D; ($n \geq 4$); Parametric ANOVA, Tukey's post hoc test was performed; * indicates significance at $p \leq 0.05$ and ** indicates significance at $p \leq 0.01$].

index of ≈0.01; <1), and IL-4 would induce them into M_2 phenotype (having high M2/M1 index of ≈5.1; >1). Additionally, M_0 populations with basal CCR7 and CD206 expression levels were normalized to M2/M1 index to 1 (from flow cytometric analysis).

When naïve macrophages were treated with leachates from SR control substrates and NOgen substrates, there were two distinct observations: i) SR control, nBG 50, and nBG-Cu all favored a pro-inflammatory bias, with M2/M1 index: ≈0.19, ≈0.21 and ≈0.41, respectively, while ii) nBG-Sr favored a regenerative or

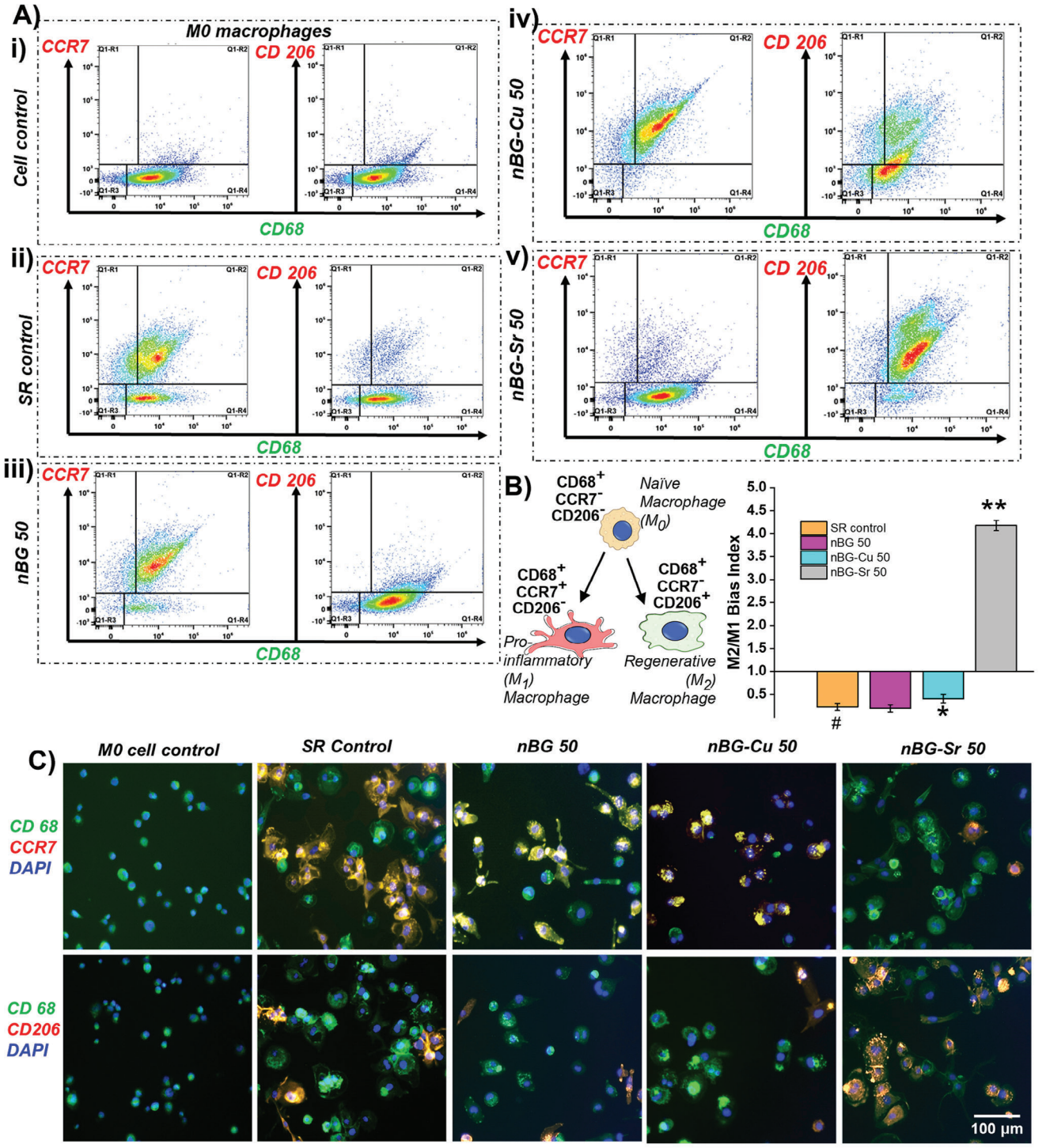

Figure 5. Effects of copper and strontium from NOgen interface leachates on macrophages. A) Flow cytometric analysis of naïve macrophages treated with 14-day leachates for 72 h to polarize them in vitro and representative dot plots for different groups are shown: i) cell control, ii) SR control, iii) nBG 50, iv) nBG-Cu 50 and v) nBG-Sr 50; and the B) M2/M1 macrophage index calculated from the populations. C) Qualitative representation of the immunostained population of macrophages treated with the leachates by fluorescent microscopy. [Data are presented as means ± S.D; ($n \geq 3$); Parametric ANOVA, Tukey's post hoc test was performed; * indicates significance at $p \leq 0.05$ and ** indicates significance at $p \leq 0.01$, in comparison to # SR control].

anti-inflammatory bias with M2/M1 index of ≈4.1 (Figure 5A,B). Qualitative assessment from immunostaining also corroborated this observation with the nBG-Sr 50 leachate-treated group having more M_2 macrophages expressing CD206, while other groups had M_1 macrophages expressing CCR7 (Figure 5C). This attests to the role of Sr as an active metal ion, which, when released at low therapeutic levels from NOgen interface, can effectively modulate the local implant site. The immunomodulatory role of Sr has been established previously in doped-bioceramic platforms used in dental or bone tissue engineering applications.[59] This is attributed to the role of Sr in decreasing the expression of COX-2,[57] whereas Cu is known to increase the level of COX-2.[29]

2.6. Immunomodulatory Effect of NOgen Interface on Macrophages

After establishing the ancillary features of metal ions from leaching, the effect of NO generated in situ from the NOgen interface was investigated to observe the fate of macrophages. The NO generation potency decreases over time (Figure S8, Electronic Supporting Information) due to the leaching/ dissolution of network modifiers (catalytic – Cu or Sr metal ions) and network formers from the amorphous bioactive glass network (Figure S7, Electronic Supporting Information). Thus, the NO flux values also decreased over time, which might affect the macrophages differently. Hence, this hypothesis was tested by performing a continuous study on the same NOgen films and their effect on polarizing at two different time points on day 3, for 72 h (exposure period of 72 h in situ generated NO) and on day 10 (exposure period of 72 h in situ generated NO) (**Figure 6A**).

Under in vitro conditions, S-nitrosothiols (such as GSNO) are unstable[36] and hence need to be supplemented frequently to maintain a steady supply of NO donors to generate nitric oxide. In generalized mathematical modeling, it took 300–400 min for a response to materialize in cells after ligand activation in receptor-mediated signal transduction, which holds true even for gasotransmitter-based signaling.[60] This was because, at every 5 h time point, the culture media was supplemented with endogenously relevant levels of 1 µM GSNO/30 µM GSH for a 72 h exposure period to study the effect of NO generated on naïve macrophages. At day-3 (Figure 6B; Figure S11, Electronic Supporting Information), all the groups favored a pro-inflammatory response, with the nBG-Cu 50 and nBG-Sr (the catalytic groups) having M2/M1 index of ≈0.02 (≪1) (potent inflammatory mediator) in comparison to SR control (M2/M1 index: ≈0.42, <1) and nBG 50 (M2/M1 index: ≈0.21, <1) (mild mediator). Interestingly, at day-10 (Figure 6C; Figure S12, Supporting Information), SR control and GSNO control maintained the same trend as day-3 (mild pro-inflammatory mediator), while nBG 50 had an M2/M1 index of ≈0.88 (close to 1, neither pro nor anti-inflammatory bias). nBG-Cu 50 maintained its potent pro-inflammatory mediator M2/M1 index at ≈0.08 (≪1), in contrast to nBG-Sr 50, which favored a potent anti-inflammatory M2/M1 index (≈2.41 ≫ 1) bias.

Qualitative assessment from immunostaining also corroborated this observation with nBG-Sr 50 and nBG-Cu NOgen groups having predominantly CCR7 expressing M_1 macrophages at day 3. Consequently, a bias switch was noted for the nBG-Sr 50 NOgen group at day-10 where CD206 expressing M_2 macrophages were present more here in comparison to other groups (Figure 6D,E). As a gasotransmitter, NO plays several crucial roles in maintaining vascular and immune homeostasis. Such a potent pleiotropically active signaling molecule regulates its diverse biological activity by virtue of its concentration and duration on its target cells and their sensitivity to it. The controversial role of this double-edged molecule, which has been extensively associated with pathological conditions, has also been proven to possess a protective effect (against ischemia and thrombosis).[61] It was observed that the NOgen groups (nBG-Cu 50, nBG-Sr 50, at day-3) produce NO concentration >2.5 nM (Figure S8 electronic Supporting Information, observed at day 1, 3; corresponding to a flux value of $>1.5 \times 10^{-10}$ mol cm^{-2} min^{-1}), and this concentration was favoring an M_1 macrophage polarization bias; whereas when the NO concentration dropped below 0.8 nM (for nBG-Sr 50, at day 7, Figure S8, Electronic Supporting Information, corresponding to flux value $<0.4 \times 10^{-10}$ mol cm^{-2} min^{-1}), a M_2 macrophage polarization bias was favored, showcasing flux-dependent immunomodulation. At lower concentrations, NO is known to activate its classical NO/sGC/cGMP (cyclic guanosine monophosphate) signaling axis,[33] however, at relatively higher concentrations, NO (>60 nM) it activates phosphoinositide 3-kinase (PI3K)[62], and mediates the phosphorylation of protein kinase B (Akt) leading to enhanced nuclear binding of transcription factor NF-κB to its inflammatory modulator sequences.[61] It has also been reported that macrophage metabolism is altered in response to NO. Pro-inflammatory stimulation (in M_1 macrophages) has been reported to switch to a high glycolytic status with the increase in lactate production; while glucose carbon flux is unaltered through tricarboxylic acid cycle (TCA) under low flux values (in M_2 macrophages).[63,64] These interesting directions need further investigation to dissect the role of NOgen interfaces in governing the macrophage phenotype through metabolism and downstream signaling pathways such as sGC/cGMP, PI3K-dependent, or TGF-β1/NFκB signaling.

For the success of any biomaterial, it should never favor only M_1 or M_2 macrophage bias; prolonged inflammation could lead to extensive fibrosis, while rapid M_2 activation could result in delayed onset of fibrosis owing to inadequate remodeling and immune cell engagement.[65,66] A delicate balance is needed, which was observed in the nBG-Sr NOgen interface, which favors pro-inflammatory bias initially and then aids in M_2 phenotype activation. Moreover, the tandem effects of metal ion release (say after 14 days) would further reduce the fibroblast activation, leading to attenuation of the fibrotic response.

2.7. Proangiogenic Effect of NOgen Interface

Neo-vascularization is critical for long-term implantable devices such as defect fillers, stents, and sensors. The formation of new capillary blood vessels helps in remodeling the tissue space at the implant site and reduces the extent of fibrous capsule formation. Strategies involving the release of growth factors (such as vascular endothelial growth factor VEGF) and anti-inflammatory drugs (like dexamethasone) from antifouling substrates have

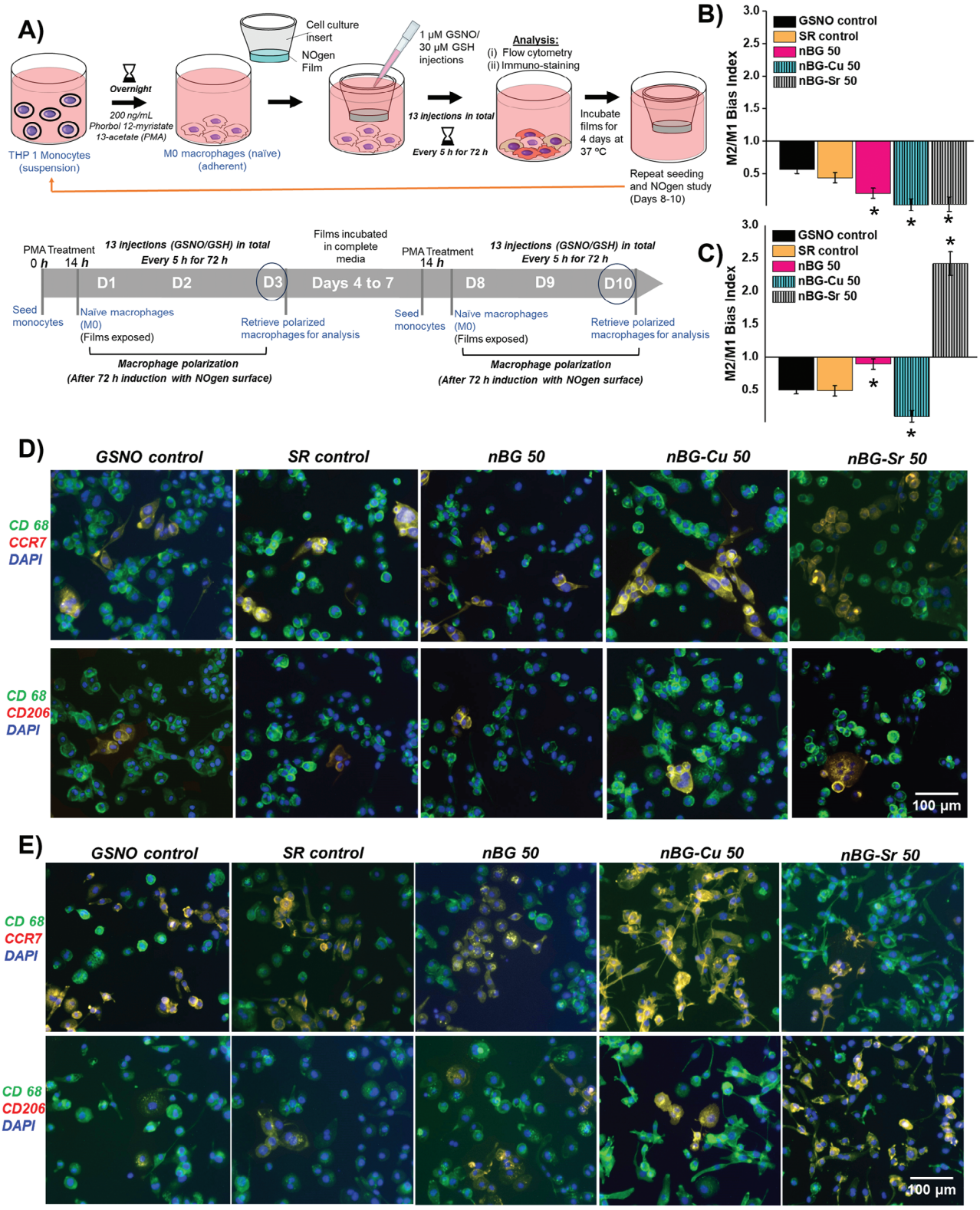

Figure 6. Effects of NOgen interface on macrophages. Immunomodulatory effect of NO generated from NOgen interface on macrophages over a period of 10 days, A) using the strategy depicted in the scheme; M2/M1 macrophage bias index calculated from the flow cytometric analysis of macrophage population retrieved at B) Day-3 and C) Day-10; Qualitative representation of the immunostained population of macrophages retrieved at D) Day-3 and E) Day-10 by fluorescent microscopy. [Data are presented as means ± S.D; ($n \geq 3$); Parametric ANOVA, Tukey's post hoc test was performed; * indicates significance at $p \leq 0.05$ in comparison to SR control].

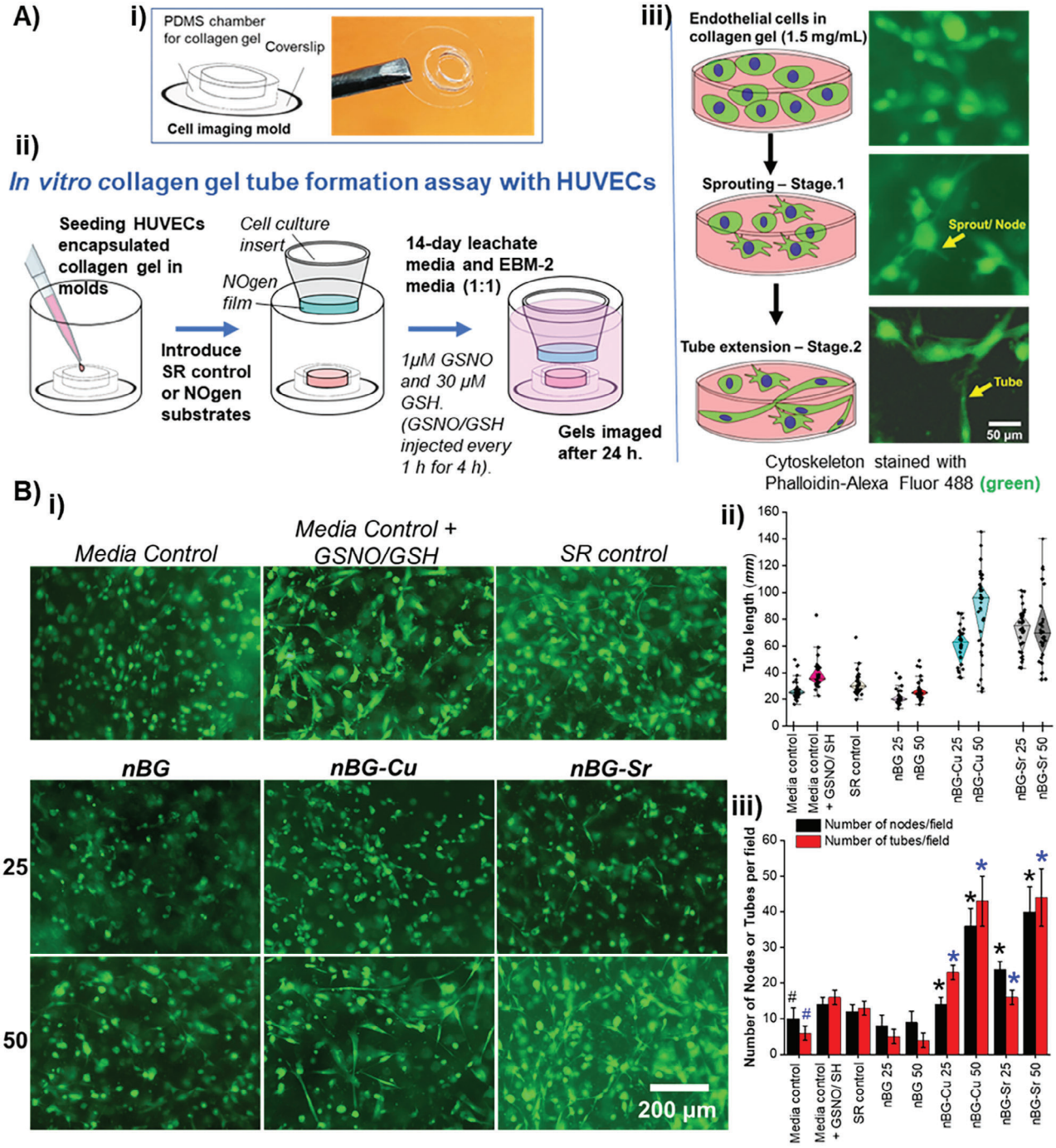

Figure 7. Proangiogenic effect of leachates and NOgen interface. A) in vitro collagen tube formation performed using human umbilical vein endothelial cells on i) custom microscope molds, following the ii) method illustrated in the scheme, and iii) assessing the number of nodes and tube length of matured endothelial cell network after staining. B) i) Fluorescent images (representative), ii) tube length measured, and iii) the number of tubes and nodes noted per frame from the images for different groups. [Data are presented as means ± S.D; ($n \geq 3$); Parametric ANOVA, Tukey's post hoc test was performed; * indicates significance at $p \leq 0.05$, in comparison to # media and SR control].

been shown to be effective in rat models.[67] Hence, the proangiogenic potential of the NOgen interface was evaluated by performing a collagen gel tube formation assay (**Figure** 7A). The collagen gel with embedded endothelial cells mimics the tissue space, which helps in quantifying the extent of nodal points and tube length of the endothelial cell network generated in response to the NO-generated and leachate treatment. An increased number of nodes/sprouts and tubes were observed in the Cu and Sr incorporated NOgen groups (with no significance noted between nBG-Cu 50 and nBG-Sr 50). Similarly, longer endothelial tubes were

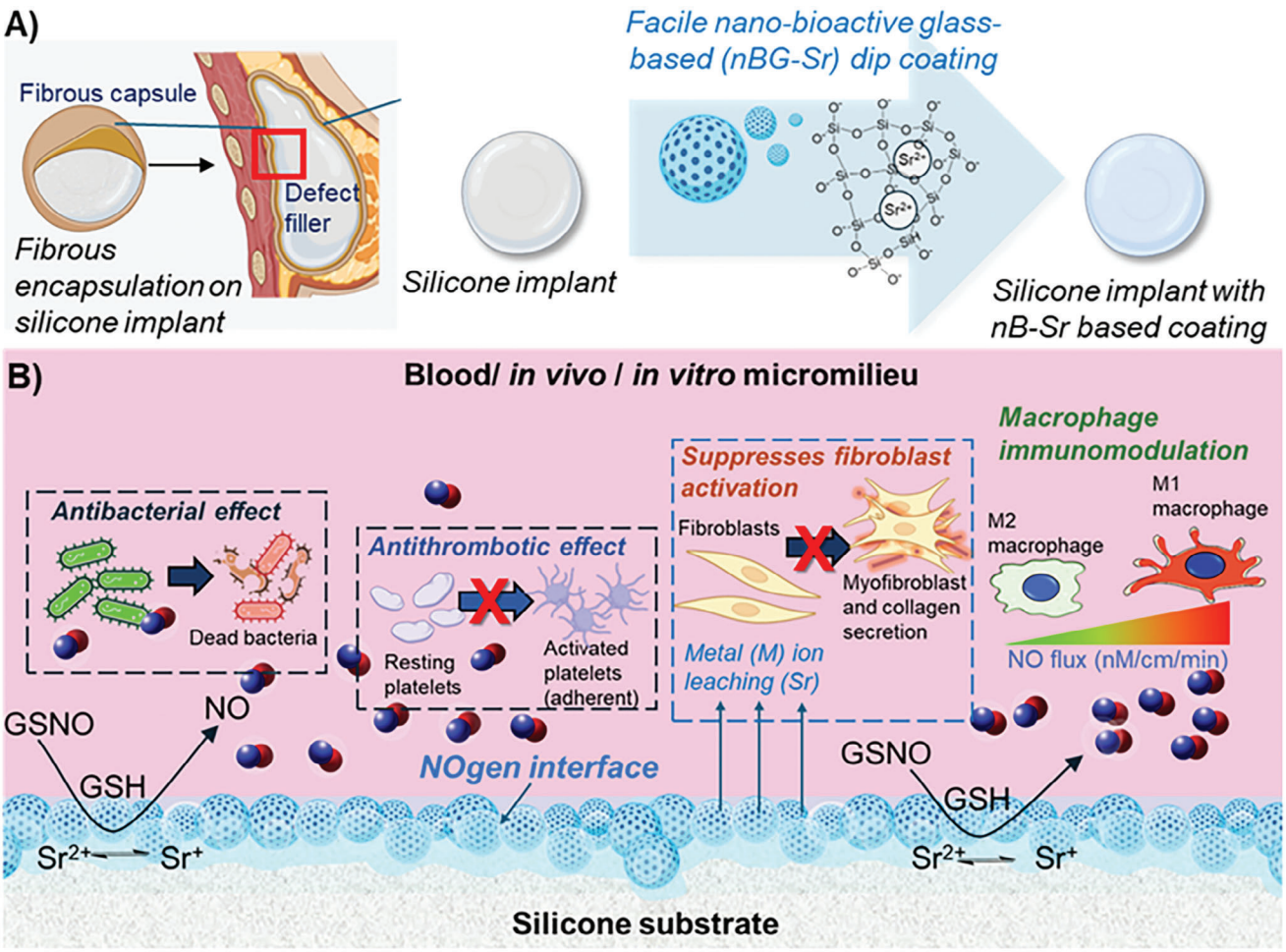

Figure 8. A) A facile strategy to develop conformal coatings of doped nano-bioactive glass on silicone substrates toward attenuating implant-associated fibrosis through in situ nitric oxide (NO) generation is presented here. B) The pleiotropic effect of NO generated exhibited antibacterial activity and decreased platelet adhesion. The NO generated in tandem with the low therapeutic release of strontium ions from the NOgen interface regulated cellular fate pertaining to fibroblasts, macrophages, and endothelial cells. Graphics were created using Biorender software.

formed in nBG-Cu 50 ad nBG-Sr 50 groups, indicating the NO generated from these interfaces facilitated the maturation of the endothelial cells, and the leachate treatment did not affect the viability of the endothelial cells (Figure S14, Electronic Supporting Information). This is in correlation to the other reports where Cu-based metal–organic framework-modified Ti surfaces (for vascular stents) aided in situ NO generation, promoting rapid reendothelialization and suppressing smooth muscle cell activity.[68]

The use of therapeutic metallic ions has gained impetus in biomaterials and tissue-engineered products owing to the convenience of their incorporation during fabrication when compared to the inclusion of organic drugs or biomolecules due to incompatibility or stability issues associated with the latter.[69] Though copper has been explored in the past for its positive effect in modulating the cardiovascular system, promoting bone fracture healing, and exerting antibacterial effects,[70] more recently, strontium is being investigated due to its favorable effects in modulating immune response.[71,72] In this work, we also probed the catalytic behavior of Sr in decomposing endogenous s-nitrosothiols for NO generation. These NOgen nBG-Sr surfaces were thus holistically investigated for their cell-instructive properties on platelets, fibroblasts, macrophages, and endothelial cells (**Figure 8**). It is obvious that NO has pleiotropic roles, and its effect on these cells had a favorable outcome, which attests to the prospects of an nBG-Sr-based NOgen interface that prevents implant-associated fibrosis. Though the current work carried out a thorough in vitro preliminary investigation, the in vivo performance of the nBG-Sr-based NOgen interfaces also needs to be validated in suitable animal models for long-term resorption kinetics roles along with the released strontium's bioactive therapeutic effects. Traditionally, NO has been known to be a potent pro-inflammatory mediator. More recently, the role of NO flux in modulating the macrophage phenotype has garnered attention.[61,73] However, most of these studies use cytokine to prime the naïve macrophages to elicit NO production,[73] or the use of NO donors (in different concentrations) such as *S*-nitroso-*N*-acetyl-DL-penicillamine and sodium nitroprusside to generate NO and study their effects on macrophages.[74] The technical limitation to precisely quantify NO (a short-lived gasotransmitter) in vitro from cells or in vivo relies on biochemical

estimation,[32,73] making it difficult to determine a NO flux /dose that can precisely modulate the immune response. In this work, we noticed NO flux value of $>1.5 \times 10^{-10}$ mol cm^{-2} min^{-1} favored M_1 macrophage polarization bias; whereas when the NO concentration dropped below 0.8 nM (for nBG-Sr 50, corresponding to flux value $<0.4 \times 10^{-10}$ mol cm^{-2} min^{-1}), it favored an M_2 macrophage polarization bias. The NO flux secreted by immune cells or endothelial cells in the human body is also subjective and depends on the homeostatic condition of the individual. Hence, a thorough analysis to assess the phenotypic switching with relation to NO flux, taking into consideration the molecular mechanisms involving several shared key mediators of inflammation, fibrosis, and angiogenesis needs to be validated. This would be essential toward establishing a correlation for developing NOgen interfaces that can tailor the cellular response more precisely to give us more insights into NO's regulatory roles along with the strontium's bioactive therapeutic effects.

3. Conclusion

In summary, herein, to attain an in situ NO generation to harness the pleiotropic effects of NO, a catalytic interface was developed using mesoporous doped-nanobioactive glass particles. The role of copper and strontium in acting as metal catalysts to decompose endogenous reservoirs of S-nitrosothiols was investigated. The facile modification of SR substrates by dip-coating them with these nanoparticles helped generate physiologically relevant levels of NO. NOgen interfaces exhibited bactericidal and antithrombotic properties. In addition to NO, these NOgen interfaces also served as active surfaces capable of releasing low therapeutic doses of copper or strontium ions, which had other ancillary cell-instructive benefits. The strontium ion from leachates suppressed the collagen expression and migration of activated fibroblasts. The NO generated from NOgen interfaces regulated the macrophages, bestowing an immunomodulatory effect. Altogether, the multifunctional NOgen interfaces developed here serve as a valuable strategy in combating implant-associated infections and attenuating implant-associated fibrosis noted in silicone-based implantable devices.

4. Experimental Section

Chemical reagents conforming to ACS reagent grade (purity ≥98%) such as hexadecyltrimethylammonium bromide (CTAB), Tris(hydroxymethyl)aminomethane (Tris base), tetraethylorthosilicate (TEOS), calcium nitrate tetrahydrate, triethylphosphaste (TEP), copper (II) chloride dihydrate, strontium chloride, hexahydrate, sodium nitrite, L-ascorbic acid, Direct red 80, triton-X 100, tween-20 and ethylenediaminetetraacetic acid (EDTA) were obtained from Millipore-Sigma (St. Louis, MO, USA); 1,10-phenanthroline was obtained from Fisher Scientific (Fair Lawn, NJ, USA). All solvents, bases, acids, and biological reagents were procured from Fisher Scientific (Fair Lawn, NJ, USA) unless otherwise mentioned differently in the subsequent text. For detailed procedures of the following methods please refer to the associated electronic Supporting Information file.

Synthesis of Mesoporous Bioactive Glass Nanoparticles: A modified Stöber's method was adopted for the synthesis of mesoporous bioactive glass belonging to the glass composition: $70SiO_2.25CaO.5P_2O_5$ using a sacrificial templating technique.[26,31] CTAB was chosen as the surfactant to form a micellar template acting as a capping agent for the dendrimeric silica network formation using TEOS as the SiO_2 (network formers) precursor to which other non-bridging oxide precursors (network modifiers) were sequentially added. Briefly, 4 mM CTAB in Tris-HCl buffer (10 mM, pH 8.0) was used to hydrolyze TEOS for 1 h at ambient conditions (25 ± 2 °C) under continuous stirring. The CaO and P_2O_5 precursors in the form of calcium nitrate tetrahydrate and TEP were subsequently added after 1 h intervals in succession to each precursor addition. The molar ratio of the constituents was maintained at 70:25:5, TEOS: calcium nitrate tetrahydrate: TEP. The reaction was allowed to continue for 48 h under stirring conditions, after which the nanobioactive glass (**nBG**) precipitates were collected by centrifugation. For the synthesis of doped bioactive glass nanoparticles, either copper-doped nanobioactive glass (**nBG-Cu**) or strontium-doped bioactive glass (**nBG-Sr**), copper (II) chloride dihydrate or strontium chloride was added after CaO precursor addition step as noted earlier for **nBG** synthesis, followed by same processing steps. The molar ratio of the constituents was maintained at 70:20:5:5, TEOS: calcium nitrate tetrahydrate: copper (II) chloride dihydrate: TEP for **nBG-Cu**, while 70:20:5:5, TEOS: calcium nitrate tetrahydrate: strontium chloride: TEP for **nBG-Sr**, respectively.

Dip Coating of Silicone Substrates to Obtain NOgen Interfaces: Medical grade silicone rubber (SR) sheets with a thickness of 1 mm (McMaster-Carr, Douglasville, GA, USA) were used as substrates for developing the NOgen interfaces. A dip coating strategy was adopted wherein RTV silicone (Dowsil RTV 3140, Midland, MI, USA) was chosen as the polymer so it could bond well with SR substrates without delamination and cured at ambient conditions. Depending on the concentration of nanoparticles in suspension, the experimental groups were denoted as nBG-Cu 5, nBG-Cu 15, nBG-Cu 25, and nBG-Cu 50 for concentrations 5, 15, 25, and 50 mg mL^{-1}, respectively (likewise for other sample types also). Control substrates (SR control) for biological experiments were made from SR (6 mm punchouts), dip coated with 200 mg mL^{-1} RTV (thrice), and a similar procedure was followed for curing and removal of any residual solvent.

Synthesis of S-nitrosoglutathione (NO donor) for NOgen Studies: GSNO was synthesized based on a previously published method[34] from reduced glutathione (GSH) (Alfa Aesar, Waltham, MA, USA). Briefly, 16 mM GSH was dissolved in 0.48 M HCl, and this mixture was cooled down in an ice bath. Excess sodium nitrate (17 mM) was added to this cooled mixture and allowed to react for 40 min. Cold acetone was added to crash out GSNO as pink precipitate which was collected by vacuum filtration. The precipitate was washed with cold acetone, followed by deionized water to remove any unreacted reagents, and dried overnight under a vacuum. The dried GSNO product was ground using mortar and pestle and stored at −20 °C until further use. The purity of the synthesized GSNO was tested using a Nitric Oxide Analyzer (NOA) and was found to be >95%.

Physicochemical Characterizations: The synthesized nanoparticles were characterized for their size, morphology, and functional composition. Hydrodynamic radius, polydispersivity index, and surface charge were analyzed by dynamic light scattering studies by Zetasizer Nano S90 (Malvern Panalytical, UK) equipped with Zeta potential measurement. Surface microstructure and compositional analysis of the synthesized nanoparticles were analyzed by a high-resolution scanning transmission electron microscope (HR-STEM, Hitachi SU9000EA, Japan) equipped with Oxford large area windowless – energy dispersive spectroscopy (EDS) and micro-electron diffraction to gather SAED detectors. The functional composition of fingerprint regions of synthesized nanoparticles was analyzed using a Fourier transform infrared spectrometer (Spectrum Two, PerkinElmer, USA).

The static water contact angle (droplet volume = 5 µL) of dip-coated NOgen substrates ($n \geq 5$), was measured using a contact angle goniometer (Ossila Ltd., UK). The metal ion leachate from the dip-coated substrates at different time points was quantified using an inductively coupled plasma optical emission spectrophotometer (ICP-OES) Perkin Elmer 8300 (PerkinElmer, USA). The nitric oxide generated from NOgen substrates was measured using Sievers chemiluminescence nitric oxide analyzer (Zysense NOA 280i, G.E. Analytical, USA).

Antibacterial Studies: The antibacterial efficacy of the NO from NOgen substrates ($n \geq 4$) was challenged against planktonic cultures of two

commonly noted bacterial strains associated with implant infections: Gram-negative, *E. coli* (ATCC 25 922) and Gram-positive *S. aureus* (ATCC 6538), which were procured from American Type Culture Collection (ATCC, VA, USA). To assess the reduction of planktonic bacteria population bacterial suspension was serially diluted and plated in LB agar plates using a spiral plater (Eddy Jet 2, IUL Instruments, Spain). Colonies were counted using an automated colony counter (Sphere Flash, IUL Instruments, Spain).

Platelet Adhesion Study: The protocol for the ethical use of freshly drawn whole porcine blood was approved by the Institutional Animal Care and Use Committee (IACUC): AUP A2023 11-123-Y1-A3. The University of Georgia Swine unit is under IACUC inspection and supervision, and all sampling procedures were followed as per the Guide for the Care and Use of Agricultural Animals in Research and Teaching by the Federation of Animal Science Societies (FASS). Platelet solution in the density of 10^8 platelets mL^{-1} was supplemented with 1 µM GSNO and 30 µM GSH (final concentration) and incubated for 90 min at 37 °C under mild rocking conditions with the substrates. The substrates were retrieved and rinsed in PBS to remove loosely adhered platelets, and the adhered platelets to substrates were detected by lactate dehydrogenase (LDH) released was quantified using Roche LDH detection kit (Millipore-Sigma, St. Louis, MO, USA).

In Vitro Biological Studies: The cell instructive facets of the NOgen substrates were tested on human fibroblasts, endothelial cells, and macrophages. For these the following cell lines were obtained: human fibroblasts (BJ, CRL-2522, ATCC, USA), human umbilical vein endothelial cells (HUVECs) (PCS-100-010, ATCC, USA), and human monocytic cell line (THP-1) (TIB-202, ATCC, USA) and maintained in their respective culture media. All consumables and biological reagents were procured from Thermo Fisher Scientific (Waltham, MA, USA).

Cytocompatibility Assessment: The cytocompatibility assessment was done following ISO standard (ISO10993-5: 2009) protocol by i) collecting leachates and ii) through indirect contact method. NOgen and SR control substrates ($n = 4$) (6 mm diameter, ≈1 mm thick) were UV sterilized before experimentation. Fibroblasts were seeded in 96 well plates (8000 cells $well^{-1}$) and after 24 h post-seeding, 100 µL of collected leachates were added as treatment (for 24 h). The relative cell viability percentage of the treated and non-treated (cell control group) were assessed using 0.5 mg mL^{-1} MTT (3-[4,5-dimethylthiazol-2-yl]-2,5 diphenyl tetrazolium bromide) reagent (Millipore-Sigma, St. Louis, MO, USA). Similarly, for the indirect contact method, 25 000 cells were seeded per well in a 24-well plate, and after 24 h post-seeding sterilized specimens were exposed to cells via a transwell insert (6.5 mm diameter polycarbonate 3 µm pore size, Millipore-Sigma, St. Louis, MO, USA). After 24 h of exposure, the relative cell viability percentage of the treated and non-treated (cell control group) were assessed using MTT assay.

In Vitro Fibrosis Assay: The effect of 14 days leachate on fibroblasts was further studied by setting up an in vitro fibrosis assay and quantifying the reduction of fibroblast activity in the presence of a known stimulant ascorbic acid.[53] Fibroblasts were seeded on 12 well plates at a seeding density of 10^5 cells $well^{-1}$, and culture media were supplemented with 100 µM ascorbic acid to stimulate collagen synthesis for 24 h. The collagen secreted by cells was quantified by Sirius Red assay using type-1 rat tail collagen (Corning, Millipore-Sigma, St. Louis, MO, USA) as standards and was read at 550 nm using a multi-plate reader (Cytation 5, BioTek, Agilent, USA).

The effect of leachate was also investigated on the migration ability of ascorbic acid-treated fibroblasts. For this purpose, two-well silicone inserts (ibidi USA, Inc., Fitchburg, WS, USA) with a gap size ≈500 µm were used in a 24-well plate. The rate of cell migration to close the gap was assessed by taking phase contrast images using a phase contrast microscope (Advanced Microscopy Group's AMG EVOS microscope, USA) at regular time intervals. The percentage closure ($n = 4$) was estimated from the phase contrast images using Image-J (National Institutes of Health, USA) software.

Macrophage Polarization Studies: Human monocyte cell line (THP-1) was cultured as suspensions in RPMI-1640 media supplemented with 10% (v/v) FBS, 0.05 mM mercaptoethanol, and penicillin-streptomycin (10 U mL^{-1} and 10 µg mL^{-1}, respectively). Monocytes in suspension were inducted into adherent naïve macrophages (M_0) by phorbol 12-myristate 13-acetate (PMA). The naïve macrophages were polarized into either pro-inflammatory (M1) or anti-inflammatory (M2) phenotype by treating them with either 20 ng mL^{-1} interferon-γ (IFN-γ) or interleukin-4 (IL-4) (Peprotech, Thermo Fisher Scientific) respectively, for 72 h. This served as the workflow for control cell experiments. For testing the effect of leachates (14-day) and the NOgen films ($n \geq 3$), THP-1 monocytes were seeded at a density of 10^5 cells per well in 24 well plates and induced to M0 macrophages by PMA treatment. Meanwhile, for testing the effect of NO from NOgen substrates, UV-sterilized substrates (6 mm diameter, ≈1 mm thickness) were exposed to M_0 macrophages using transwell inserts (6.5 mm polycarbonate 3 µm pore size) in 1 mL of monocyte culture media with 1 µM GSNO and 30 µM GSH injections supplemented every 5 h for 72 h (13 injections in total). The macrophages obtained on day-3 and day-10 were subsequently analyzed.

The polarized macrophages were trypsinized and characterized for the population distribution using flow cytometry by staining for mouse monoclonal against human CD 68 (pan macrophage marker) and rabbit polyclonal against human CCR7 (pro-inflammatory marker M_1) and rabbit polyclonal against human CD 206 (anti-inflammatory marker M_2). The cells stained with a secondary antibody cocktail consisting of Alexa Fluor 488 conjugated goat-anti mouse Ig and Alexa Fluor 647 conjugated-donkey-anti rabbit Ig and were analyzed in a flow cytometer (Cytek Aurora, Cytek Biosciences, USA). Immunocytochemistry using the same antibodies was performed to qualitatively assess polarized macrophages. The stained cells were washed with PBS (pH 7.4) with 0.1% (v/v) tween-20 and imaged using a fluorescence microscope (AMG EVOS-FL, USA).

In Vitro Angiogenesis Assay: HUVECs were maintained in endothelial cell growth media (Lonza EGM-2) supplemented with its bullet kit components (Lonza Lifescience, Walkersville, MD, USA). Type-1 rat tail collagen was used as the basement substrate to encapsulate HUVECs and the extent of sprouting (node formation) and tube extension within the collagen gel was studied by staining the F-actin cytoskeleton. The stained endothelial tube network was imaged using a fluorescence microscope (AMG EVOS-FL, USA). The fluorescent images were analyzed using Image-J software to estimate the number of endothelial nodes and the tube length.

Statistical Analysis: All the experiments were performed in biological or technical replicates ($n \geq 3$), unless otherwise noted in the respective Experimental Section and the results were represented as mean ± standard deviation (mean ± SD). One-way analysis of variance (ANOVA) via Tukey's test was performed on parametric data sets using Origin 2018b graphing and analysis software (OriginLabs, USA) to analyze the statistical significance and the results between two test groups were considered statistically significant if the *p*-value was found to be less than 0.5.

Supporting Information

Supporting Information is available from the Wiley Online Library or from the author.

Acknowledgements

This work was supported by the National Institutes of Health through the funds received under NIH R01HL157587. The technical assistance provided by Sarah C. Jantzi, Plasma Chemistry Laboratory at the Centre for Applied Isotope Studies, University of Georgia for ICP-OES analysis; and Juan M. Bustamante, CSRL Cytometry Shared Resource Laboratory, University of Georgia for flow-cytometry analysis are greatly appreciated. Graphic elements in Figures 3, 8 and Table of Content illustration were created in part using Biorender software (Biorender.com). J.C.M. and A.S. contributed equally to this work.

Conflict of Interest

The authors declare the following competing financial interest(s): Hitesh Handa and Elizabeth J. Brisbois are cofounders and maintain a financial

interest in a startup company investigating nitric oxide as a biomedical therapeutic for medical devices.

Author Contributions

J.C.M., A.S., Y.W., and I.V.M. contributed to study conceptualization, conducted the experiments, and were involved in data curation, formal analysis, and writing the original draft. H.H. and E.J.B. conceived and supervised the study. H.H. and E.J.B. acquired the financial funding for the work.

Data Availability Statement

The data that support the findings of this study are available from the corresponding author upon reasonable request.

Keywords

antithrombogenic, copper, immunomodulation, nitric oxide, strontium

Received: December 10, 2024
Revised: January 24, 2025
Published online: February 24, 2025

[1] P. S. Stewart, T. Bjarnsholt, *Clin. Microbiol. Infect.* **2020**, *26*, 1034.
[2] S. Farah, J. C. Doloff, P. Müller, A. Sadraei, H. J. Han, K. Olafson, K. Vyas, H. H. Tam, J. Hollister-Lock, P. S. Kowalski, M. Griffin, A. Meng, M. McAvoy, A. C. Graham, J. McGarrigle, J. Oberholzer, G. C. Weir, D. L. Greiner, R. Langer, D. G. Anderson, *Nat. Mater.* **2019**, *18*, 892.
[3] B. H. Shin, B. H. Kim, S. Kim, K. Lee, Y. B. Choy, C. Y. Heo, *Biomater. Res.* **2018**, *22*, 37.
[4] R. Schuster, J. S. Rockel, M. Kapoor, B. Hinz, *Immunol. Rev.* **2021**, *302*, 126.
[5] T. Rhen, J. A. Cidlowski, *N. Engl. J. Med.* **2005**, *353*, 1711.
[6] M. Attur, R. Patel, G. Thakker, P. Vyas, D. Levartovsky, P. Patel, S. Naqvi, R. Raza, K. Patel, D. Abramson, *Inflammation Res.* **2000**, *49*, 20.
[7] B. Baral, M. Mozafari, *ACS Pharmacol. Transl. Sci.* **2020**, *3*, 373.
[8] Y. Gao, Q. Ma, *Smart Med.* **2022**, *1*, 20220012.
[9] M. Lam, V. Migonney, C. Falentin-Daudre, *Acta Biomater.* **2021**, *121*, 68.
[10] J. U. Park, J. Ham, S. Kim, J.-H. Seo, S.-H. Kim, S. Lee, H. J. Min, S. Choi, R. M. Choi, H. Kim, S. Oh, J. A. Hur, T. H. Choi, Y. Lee, *Acta Biomater.* **2014**, *10*, 4217.
[11] J. Ham, Y. Kim, T. An, S. Kang, C. Ha, M. Wufue, Y. Kim, B. Jeon, S. Kim, J. Kim, *ACS Appl. Mater. Interfaces* **2020**, *12*, 30198.
[12] N. G. Welch, D. A. Winkler, H. Thissen, *Adv. Drug Delivery Rev.* **2020**, *167*, 109.
[13] X. Zhou, H. Hao, Y. Chen, W. Cao, Z. Zhu, Y. Ni, Z. Liu, F. Jia, Y. Wang, J. Ji, Z. Peng, *Bioact. Mater.* **2024**, *34*, 482.
[14] M. S. Birajdar, B. H. Kim, C. Sutthiwanjampa, S. H. Kang, C. Y. Heo, H. Park, *J. Ind. Eng. Chem.* **2020**, *89*, 128.
[15] A. H. Morris, R. S. Mahal, J. Udell, M. Wu, T. R. Kyriakides, *Adv. Healthcare Mater.* **2017**, *6*, 1700370.
[16] E. M. Hetrick, H. L. Prichard, B. Klitzman, M. H. Schoenfisch, *Biomaterials* **2007**, *28*, 4571.
[17] M. Douglass, S. Hopkins, M. K. Chug, G. Kim, M. R. Garren, M. Ashcraft, D. T. Nguyen, N. Tayag, H. Handa, E. J. Brisbois, *ACS Appl. Mater. Interfaces* **2021**, *13*, 52425.
[18] M. K. Chug, E. J. Brisbois, *ACS Mater. Au* **2022**, *2*, 525.
[19] F. Rong, Y. Tang, T. Wang, T. Feng, J. Song, P. Li, W. Huang, *Antioxidants* **2019**, *8*, 556.
[20] B. K. Oh, M. E. Meyerhoff, *J. Am. Chem. Soc.* **2003**, *125*, 9552.
[21] B. Gaston, J. Reilly, J. M. Drazen, J. Fackler, P. Ramdev, D. Arnelle, M. E. Mullins, D. J. Sugarbaker, C. Chee, D. J. Singel, *Proc. Natl. Acad. Sci. U. S. A.* **1993**, *90*, 10957.
[22] E. Nagababu, J. M. Rifkind, in *Nitric Oxide: Methods and Protocols*, Springer, Totowa, NJ **2010**, pp. 27–37.
[23] M. E. Douglass, M. J. Goudie, J. Pant, P. Singha, S. Hopkins, R. Devine, C. W. Schmiedt, H. Handa, *ACS Appl. Bio Mater.* **2019**, *2*, 2539.
[24] A. Lutzke, A. C. Melvin, M. J. Neufeld, C. L. Allison, M. M. Reynolds, *Nitric Oxide* **2019**, *84*, 16.
[25] S. Gupta, S. Majumdar, S. Krishnamurthy, *J. Controlled Release* **2021**, *335*, 481.
[26] J. C. Moses, B. B. Mandal, *ACS Appl. Mater. Interfaces* **2022**, *14*, 14961.
[27] S. Lin, W. Van den Bergh, S. Baker, J. R. Jones, *Acta Biomater.* **2011**, *7*, 3606.
[28] Q. Hu, Y. Li, N. Zhao, C. Ning, X. Chen, *Mater. Lett.* **2014**, *134*, 130.
[29] K. Stachowicz, *J. Trace Elem. Med. Biol.* **2023**, *79*, 127226.
[30] I. Cacciotti, *J. Mater. Sci.* **2017**, *52*, 8812.
[31] N. Gupta, D. Santhiya, A. Aditya, *J. Mater. Chem. B* **2016**, *4*, 7605.
[32] A. Hosseinnejad, N. Ludwig, S. Mersmann, P. Winnerbach, C. Bleilevens, R. Rossaint, J. Rossaint, S. Singh, *Small* **2023**, *19*, 2205185.
[33] G. Cirino, V. Vellecco, M. Bucci, *Br. J. Pharmacol.* **2017**, *174*, 4021.
[34] A. Sapkota, A. Mondal, M. K. Chug, E. J. Brisbois, *J. Biomed. Mater. Res., Part A* **2023**, *111*, 1627.
[35] B. J. Rousseau, A. V. Soudackov, R. R. Tuttle, M. M. Reynolds, R. G. Finke, S. Hammes-Schiffer, *J. Am. Chem. Soc.* **2023**, *145*, 10285.
[36] D. Lyn H áWilliams, *J. Chem. Soc., Perkin Trans.* **1996**, *2*, 481.
[37] M. Neykov, T. van Almsick, G. Dimitrov, *J. Inorg. Gen. Chem.* **2006**, *632*, 1554.
[38] R. J. Singh, N. Hogg, J. Joseph, B. Kalyanaraman, *J. Biol. Chem.* **1996**, *271*, 18596.
[39] E. Ozkan, A. Mondal, M. Douglass, S. P. Hopkins, M. Garren, R. Devine, R. Pandey, J. Manuel, P. Singha, J. Warnock, H. Handa, *J. Colloid Interface Sci.* **2022**, *608*, 1015.
[40] B. Wang, T. Jin, Y. Han, C. Shen, Q. Li, J. Tang, H. Chen, Q. Lin, *Int. J. Polym. Mater. Polym. Biomater.* **2016**, *65*, 55.
[41] W. Peng, P. Liu, X. Zhang, J. Peng, Y. Gu, X. Dong, Z. Ma, P. Liu, J. Shen, *Chem. Eng. J.* **2020**, *398*, 125663.
[42] A. Mondal, P. Singha, M. Douglass, L. Estes, M. Garren, L. Griffin, A. Kumar, H. Handa, *ACS Appl. Mater. Interfaces* **2021**, *13*, 43892.
[43] M. G. Espey, K. M. Miranda, M. Feelisch, J. Fukuto, M. B. Grisham, M. P. Vitek, D. A. Wink, *Ann. N. Y. Acad. Sci.* **2000**, *899*, 209.
[44] R. Devine, M. J. Goudie, P. Singha, C. Schmiedt, M. Douglass, E. J. Brisbois, H. Handa, *ACS Appl. Mater. Interfaces* **2020**, *12*, 20158.
[45] P. J. Walsh, S. A. Clarke, M. Julius, P. B. Messersmith, *Sci. Rep.* **2017**, *7*, 14138.
[46] P. Hao, Y. Wang, X. Sun, J. Wang, L. W. Zhang, *Toxicol. Ind. Health* **2022**, *38*, 819.
[47] L. M. Gaetke, C. K. Chow, *Toxicology* **2003**, *189*, 147.
[48] S. Dahl, P. Allain, P. Marie, Y. Mauras, G. Boivin, P. Ammann, Y. Tsouderos, P. Delmas, C. Christiansen, *Bone* **2001**, *28*, 446.
[49] A. L. Magno, B. K. Ward, T. Ratajczak, *Endocr. Rev.* **2011**, *32*, 3.
[50] W. H. De Jong, J. W. Carraway, C. Liu, C. Fan, J. Liu, A. P. Turley, T. S. Rollins, K. P. Coleman, *Toxicol. In Vitro* **2020**, *69*, 104995.
[51] R. L. W. Messer, J. E. Doeller, D. W. Kraus, L. C. Lucas, *J. Biomed. Mater. Res.* **2000**, *50*, 598.
[52] J. C. Moses, S. K. Nandi, B. B. Mandal, *Adv. Healthcare Mater.* **2018**, *7*, 1701418.
[53] Y. Kishimoto, N. Saito, K. Kurita, K. Shimokado, N. Maruyama, A. Ishigami, *Biochem. Biophys. Res. Commun.* **2013**, *430*, 579.

[54] I. Garcıá-Ruiz, P. de la Torre, T. Dıaz, E. Esteban, I. Fernández, T. Muñoz-Yagüe, J. A. Solıś-Herruzo, *J. Biol. Chem.* **2002**, *277*, 30551.
[55] A. Córdoba, M. Satué, M. Gómez-Florit, M. Hierro-Oliva, C. Petzold, S. P. Lyngstadaas, M. L. González-Martín, M. Monjo, J. M. Ramis, *Adv. Healthcare Mater.* **2015**, *4*, 540.
[56] M. Abdelrahim, S. Safe, *Mol. Pharmacol.* **2005**, *68*, 317.
[57] R. Sun, J. Zhu, K. Sun, L. Gao, B. Zheng, J. Shi, *Int. J. Med. Sci.* **2023**, *20*, 1679.
[58] A. H. Györfi, A.-E. Matei, J. H. Distler, *Matrix Biol.* **2018**, *68*, 8.
[59] T. Li, H. He, Z. Yang, J. Wang, Y. Zhang, G. He, J. Huang, D. Song, J. Ni, X. Zhou, *Biomater. Sci.* **2021**, *9*, 2931.
[60] H. Shankaran, H. Resat, H. S. Wiley, *PLoS Comput. Biol.* **2007**, *3*, e101.
[61] Q. Hu, J. Shi, J. Zhang, Y. Wang, Y. Guo, Z. Zhang, *Adv. Ther.* **2021**, *4*, 2100032.
[62] M. L. Sheu, K. F. Chao, Y. J. Sung, W. W. Lin, S. Y. Lin-Shiau, S. H. Liu, *Cell. Signalling* **2005**, *17*, 975.
[63] V. Vijayan, P. Pradhan, L. Braud, H. R. Fuchs, F. Gueler, R. Motterlini, R. Foresti, S. Immenschuh, *Redox Biol.* **2019**, *22*, 101147.
[64] E. M. Palmieri, C. McGinity, D. A. Wink, D. W. McVicar, *Metabolites* **2020**, *10*, 429.
[65] H. M. Rostam, L. E. Fisher, A. L. Hook, L. Burroughs, J. C. Luckett, G. P. Figueredo, C. Mbadugha, A. C. Teo, A. Latif, L. Kämmerling, *Matter* **2020**, *2*, 1564.
[66] T. A. Wynn, K. M. Vannella, *Immunity* **2016**, *44*, 450.
[67] L. W. Norton, H. E. Koschwanez, N. A. Wisniewski, B. Klitzman, W. M. Reichert, *J. Biomed. Mater. Res., Part A* **2007**, *81A*, 858.
[68] Y. Fan, Y. Zhang, Q. Zhao, Y. Xie, R. Luo, P. Yang, Y. Weng, *Biomaterials* **2019**, *204*, 36.
[69] V. Mourino, J. P. Cattalini, A. R. Boccaccini, *J. R. Soc., Interface* **2012**, *9*, 401.
[70] P. Wang, Y. Yuan, K. Xu, H. Zhong, Y. Yang, S. Jin, K. Yang, X. Qi, *Bioact. Mater.* **2021**, *6*, 916.
[71] H. Li, L. Ma, *J. Mater. Chem. B* **2024**, *12*, 8267.
[72] K. Zheng, W. Niu, B. Lei, A. R. Boccaccini, *Acta Biomater.* **2021**, *133*, 168.
[73] V. Somasundaram, A. C. Gilmore, D. Basudhar, E. M. Palmieri, D. A. Scheiblin, W. F. Heinz, R. Y. Cheng, L. A. Ridnour, G. Altan-Bonnet, S. J. Lockett, *Redox Biol.* **2020**, *28*, 101354.
[74] C.-Y. Li, G. Anuraga, C.-P. Chang, T.-Y. Weng, H.-P. Hsu, H. D. K. Ta, P.-F. Su, P.-H. Chiu, S.-J. Yang, F.-W. Chen, *J. Exp. Clin. Cancer Res.* **2023**, *42*, 22.

